Gondwana Research 24 (2013) 648–663

Contents lists available at SciVerse ScienceDirect

Gondwana Research

journal homepage: www.elsevier.com/locate/gr

Mid-Silurian back-arc spreading at the northeastern margin of Gondwana: The Dapingzhang dacite-hosted massive sulfide deposit, Lancangjiang zone, southwestern Yunnan, China

Bernd Lehmann [a,b,*], Xinfu Zhao [c], Meifu Zhou [c], Andao Du [d], Jingwen Mao [d], Pusheng Zeng [d], Friedhelm Henjes-Kunst [e], Klaus Heppe [f]

[a] Mineral Resources, Technical University of Clausthal, 38678 Clausthal-Zellerfeld, Germany
[b] State Key Laboratory of Ore Deposit Geochemistry, Guiyang 550002, China
[c] Department of Earth Sciences, University of Hong Kong, Hong Kong, China
[d] Institute of Mineral Deposits, Chinese Academy of Geological Sciences, Beijing 100037, China
[e] Bundesanstalt für Geowissenschaften und Rohstoffe, 30655 Hannover, Germany
[f] Teck Exploraciones Mineras Chile Ltda., Santiago, Chile

ARTICLE INFO

Article history:
Received 17 September 2012
Received in revised form 27 December 2012
Accepted 29 December 2012
Available online 19 January 2013

Handling Editor: M. Santosh

Keywords:
VHMS
Gondwana break-up
Dapingzhang
Yunnan
South China

ABSTRACT

The Dapingzhang dacite-hosted volcanogenic massive sulfide deposit is located in a late Paleozoic collisional zone, the Sanjiang fold-and-thrust belt, characterized by a collage of Gondwana-derived terranes at the southern margin of the South China (Yangtze) block. This area has experienced repeated Paleozoic and Mesozoic collisional and extensional events, and is overprinted by Himalayan strike-slip and thrust movements. The Dapingzhang orebody is strongly sheared into discontinuous ore lenses and blocks, and is hosted by a several-hundred-meter-thick volcanic rock sequence of dacite, with minor metabasalt (spilite), rhyolite, and chert. Bulk-rock Nd isotope data give ε_{Nd} (429 Ma) values of +2 to +5, and indicate a dominantly mantle source, or origin from young continental crust (T_{DM} ~800–1000 Ma). The dacites have distinctly low abundances of Ti, Nb, Ta, Zr, Th, and REEs, which is typical of subduction-related volcanism.

The base-metal mineralization occurs as polymetallic massive sulfide mineralization, mainly pyrite, sphalerite, galena, chalcopyrite, tetrahedrite–tennantite, and locally barite, and as pyrite–chalcopyrite stockworks. Pervasive hydrothermal alteration is dominantly quartz–sericite. Maximum enrichment in gold, bismuth, selenium, and tellurium is at the interface between the stockwork and massive sulfide mineralization styles. Deeper parts of the stockwork zone are characterized by elevated molybdenum and rhenium, whereas the distal parts to the massive sulfide mineralization have high mercury, antimony, zinc, cadmium, arsenic, lead and silver. The metal association and mineral assemblage are typical of volcanic rock-hosted massive sulfides in back-arc volcanic settings.

Uranium–Pb dating on zircon by LA-ICP-MS defines an age of 429 ± 3 Ma (2σ) (n = 19) for the dacite sequence. Rhenium–Os isotope data on Mo-rich bulk ore samples define an isochron of 429 ± 10 Ma (2σ) (n = 9; MSWD 0.21; initial $^{187}Os/^{188}Os$ 3.1 ± 1.9). Common Os is very low, and the absolute abundances of ^{187}Re and ^{187}Os define a model age of 429 ± 4 Ma (n = 9; 95% confidence). The mid-Silurian dacite sequence and associated massive sulfide mineralization identify a hitherto unknown early rifting and back-arc seafloor spreading event at the northeastern Gondwana margin related to the early evolution of the Paleotethys Ocean.

© 2013 International Association for Gondwana Research. Published by Elsevier B.V. All rights reserved.

1. Introduction

The North China, South China, and Tarim blocks, and several terranes of Indochina were located along the Indo-Australian margin of northeastern Gondwana in the early Paleozoic (Metcalfe, 1998, 2005, 2006). Close faunal affinities suggest continental contiguity of these blocks with each other and with Gondwana in the Cambrian to Silurian (Rong et al., 1995). Tectono-stratigraphic, paleontological, and paleomagnetic data suggest that the blocks and terranes forming eastern and southeast Asia were then successively rifted since the Silurian and migrated northward from Gondwana in three major continental slivers in the Early Devonian (North China, South China, Tarim, Indochina, East Malaya, West Sumatra blocks), Lower Permian (Sibumasu, Qiangtang blocks), and the Late Triassic–Late Jurassic (Lhasa, West Burma blocks), respectively. Successive ocean basins opened (and subsequently closed) between each sliver and Gondwana, i.e. the Paleo-Tethys, Meso-Tethys, and Ceno-Tethys, respectively (Metcalfe, 1998, 2011).

* Corresponding author at: Mineral Resources, Technical University of Clausthal, 38678 Clausthal-Zellerfeld, Germany. Tel.: +49 5323 722776.
E-mail address: bernd.lehmann@tu-clausthal.de (B. Lehmann).

1342-937X/$ – see front matter © 2013 International Association for Gondwana Research. Published by Elsevier B.V. All rights reserved.
http://dx.doi.org/10.1016/j.gr.2012.12.018

We here report on hitherto unknown mid-Silurian dacite volcanism and associated volcanic-hosted massive sulfide (VHMS) mineralization at Dapingzhang in the Lancangjiang zone of the Yunnan province in South China, which is a part of the Simao terrane of the Indochina block at the southern margin of the South China block (Fig. 1). The mineralization is taken as an indicator of rifting and arc/back-arc volcanism. The volcanic host-rock sequence was previously assumed to have a Carboniferous age and is mapped as such in the regional geological maps of various scales (YBGMR, 1990, 2001). Our new zircon U–Pb dates for the dacitic host rocks and Re–Os isotopic ages of bulk-rock massive sulfide indicate that they formed in the mid-Silurian. Thus, the Dapingzhang deposit and its volcanic host-rock sequence document the so far known earliest episode of rifting and seafloor spreading at the northeastern margin of Gondwana.

The Dapingzhang dacite sequence and associated massive sulfide mineralization is much different in time and geotectonic setting from other massive sulfide deposits in western Yunnan, such as in the Changning–Menglian belt west of the Simao terrane. The massive sulfide deposits in the Changning–Menglian belt are of Early Carboniferous age and their host rocks are dominantly alkalic basalts related to back-arc spreading during the amalgamation of the SE Asian terrane collage and closure of the Paleotethys ocean(s) (Yang et al., 1999). In contrast, the older Dapingzhang sequence documents the incipient fragmentation of Gondwana related to subduction of the Paleo-Pacific Ocean, which was followed by successive terrane dispersal, and reassembly in the SE Asian terrane collage.

2. Geological setting

The Lancangjiang (Lancang river) zone of southwestern Yunnan is part of the Paleotethys orogenic belt in southwestern China and southeast Asia (Zhong, 1998). It is characterized by the amalgamation of a number of Gondwana-derived continental fragments, i.e. the group of continental blocks which separated from Indo-Australian Gondwana in the Devonian (the large blocks of South China and Indochina, with the Simao block as a sub-terrane of the Indochina block), and the group of continental blocks which separated from Gondwana in the Early Permian (Tengchong, and Sibumasu, with the Baoshan block as part of the Sibumasu block (Metcalfe, 2006, 2011)) (Fig. 1). The two groups of blocks are bounded by the Changning–Menglian suture zone which represents the main consumption zone of the Paleo-Tethys Ocean which was closed during the Late Permian to Triassic collision of the two groups of blocks (Metcalfe, 2006, 2011).

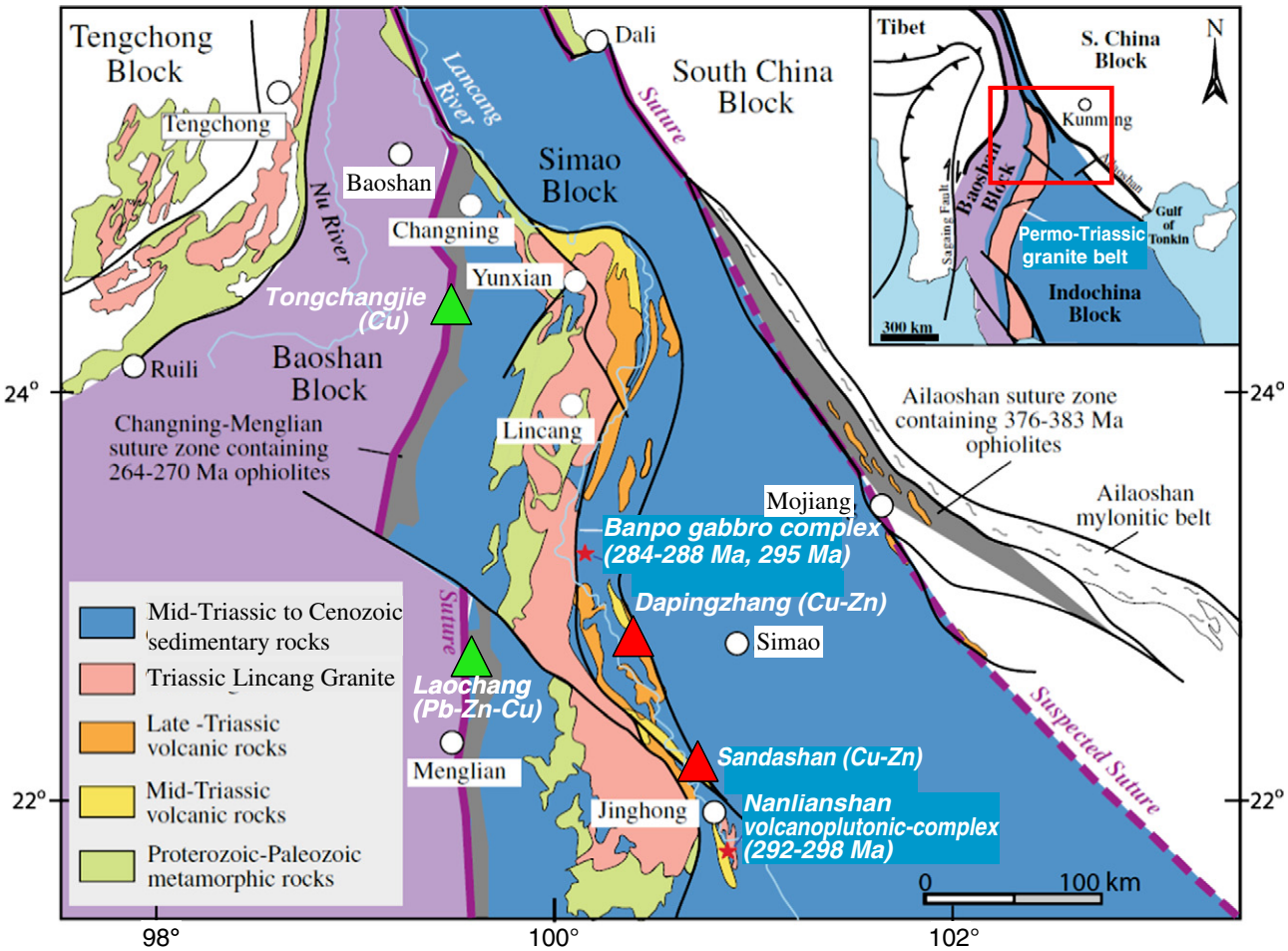

Fig. 1. Location of the Dapingzhang volcanic-hosted massive sulfide (VHMS) deposit (red triangle) in the Simao block of the Sanjiang (Three River) foldbelt between the South China block (Yangtze Platform) to the east and the Baoshan block to the west. Suture lines mark the boundaries between different Gondwana-derived terranes. The ~240 Ma late-tectonic to post-collisional Lincang Granite and volcanic rocks mark the major magmatic front of the amalgamation of the Indochina (including Simao) and Sibumasu (including Baoshan) composite terranes in the Triassic. Several mafic–ultramafic complexes, such as the Nanlianshan and Banpo gabbro intrusions, indicate eastward subduction under the Indochina block as early as about 290 Ma (Hennig et al., 2009; Jian et al., 2009a, 2009b; Li et al., 2012). Note that the mafic-dominated Laochang and Tongchangjie VHMS deposits (green triangles) in the Changning–Menglian suture zone west of the Lincang Granite are of Carboniferous age and related to a back-arc setting during the Permo-Carboniferous closure of the Paleotethys Ocean (Yang et al., 1999). The Sandashan VHMS deposit, about 60 km south of Dapingzhang, has some features similar to Dapingzhang, but reliable geological information is missing. Geology generalized from YBGMR (1990), and adapted from Li et al. (2012).

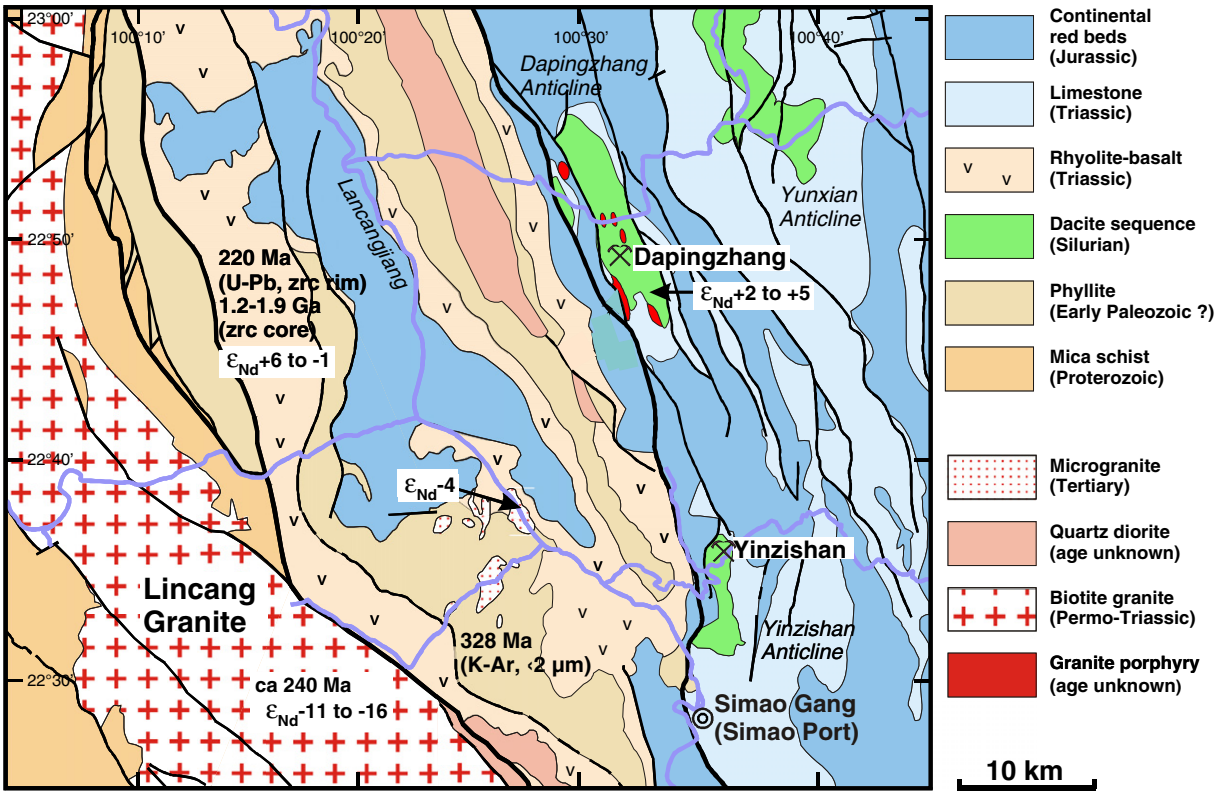

Fig. 2. Geological map of the Dapingzhang area based on YBGMR (2001). The Dapingzhang massive sulfide/stockwork deposit and the smaller satellite deposit of Yinzishan are hosted in a mid-Silurian dacite sequence (ca 429 Ma) that is exposed in the core of NW-trending anticlinal horst structures. Whole-rock epsilon Nd data are recalculated to magmatic ages and indicate a mainly mantle source for the mid-Silurian dacite sequence, as well as for the Permo-Triassic continental rift-related rhyolite-basalt volcanism. This is in contrast to the syn- to post-orogenic Triassic Lincang granite belt, which has an origin from Proterozoic basement. The bulk-rock dacite sample Y-1 used for U–Pb dating of zircon is from about 1000 m east of the Yinzishan mine along the Simao–Lincang highway.
Data from Heppe (2006), Heppe et al. (2007), and this study.

The region is known as Sanjiang (Three river) fold-and-thrust belt, as defined by three regional shear zones morphologically accentuated by the course of the Jinshajiang (Red river/Ailaoshan shear zone), Lancangjiang (Lancang river, downstream known as Mekong river) and Nujiang (Nu river fault zone) (Fig. 1). These fault zones with a sigmoidal northwest- to north-trending geometry represent Cenozoic and still active strike-slip zones with displacement rates of several hundred km. They are related to escape tectonics from the collision of India with the Asian continent (Tapponnier et al., 1990; Wang and Burchfiel, 1997). These major fault zones separate terranes of Gondwana-derived continental affinity, with disrupted remnants of oceanic crust preserved in the fault zones. The Janshajiang–Ailaoshan fault zone is characterized by gabbro, anorthosite, and MORB dated at 387–374 Ma (Jian et al., 2009a). The Lancangjiang fault zone includes the Banpo mafic–ultramafic complex dated at 288–284 Ma (Jian et al., 2009a) or 295 Ma (Li et al., 2012), and the Nanlianshan mafic–ultramafic volcanoplutonic complex dated at 298–292 Ma (Hennig et al., 2009; Li et al., 2012). The Permian Changning–Menglian ophiolite zone to the west (ca. 270–264 Ma; Feng, 2002; Jian et al., 2009a) is generally regarded as marking the main Paleo-Tethys suture between the first set of continental blocks which separated from Gondwana in the Early Devonian, and the second set of continental blocks which separated from Gondwana in the Early Permian, with the Paleo-Tethys Ocean in between.

The Early Triassic final closure of the Paleo-Tethyan Ocean(s) is indicated by the intrusion of the regionally distributed ca. 240–230 Ma Triassic Lincang granite belt (Peng et al., 2006; Hennig et al., 2009). The Permo-Triassic basin closure and collision was accompanied by an eastward progressing fold-and-thrust deformation front with a westward increase in intensity from very-low-grade to blueschist facies (high-P/low-T metamorphism) west of the Lincang granite belt, with local granulite facies metamorphism surrounding the Lincang granite batholith (Zhang et al., 1993). The Triassic Lincang granite belt marks the magmatic front (sensu Sengör et al., 1993) of the eastward subduction (according to present-day geography) of the Paleo-Tethys Ocean and collision of the major Indochina and Sibumasu blocks. This peraluminous, ilmenite-series granite belt can be traced into Peninsular Malaysia and the Java Sea, and has a Paleoproterozoic protolith ($\varepsilon_{Nd} \leq 10$; Liew and McCulloch, 1985; Heppe, 2006; Peng et al., 2006; Hennig et al., 2009). Its emplacement and exhumation is accompanied by post-orogenic relaxation with rifting, bimodal volcanism, and continental sedimentation.

Permian to Triassic basalts along the Lancangjiang fault zone have intracontinental chemical characteristics similar to synchronous flood basalts from the Emeishan LIP, which is located a few hundred kilometers to the north (Heppe, 2006; Jian et al., 2009a, 2009b). The 258 Ma Paleng mafic/ultramafic intrusion south of Jinghong and close to the Lao border also has Emeishan features (Hennig, 2010). Regional extension characterizes the Jurassic to Paleogene evolution, with exhumation of the Lincang granites and their country rocks west of the Lancangjiang, and deposition of several kilometers of continental red-beds east of the Lancangjiang (Simao basin). The Simao basin was inverted in the Eocene, with complex thrusting, folding, faulting, and rotation as a consequence of the transtensional events of the India–Asia collision in western Yunnan (Wang and Burchfiel, 1997).

3. Local geology

The Dapingzhang deposit, about 30 km north of Simaogang (Simao Port), is located along the margin of the Mesozoic–Cenozoic Simao

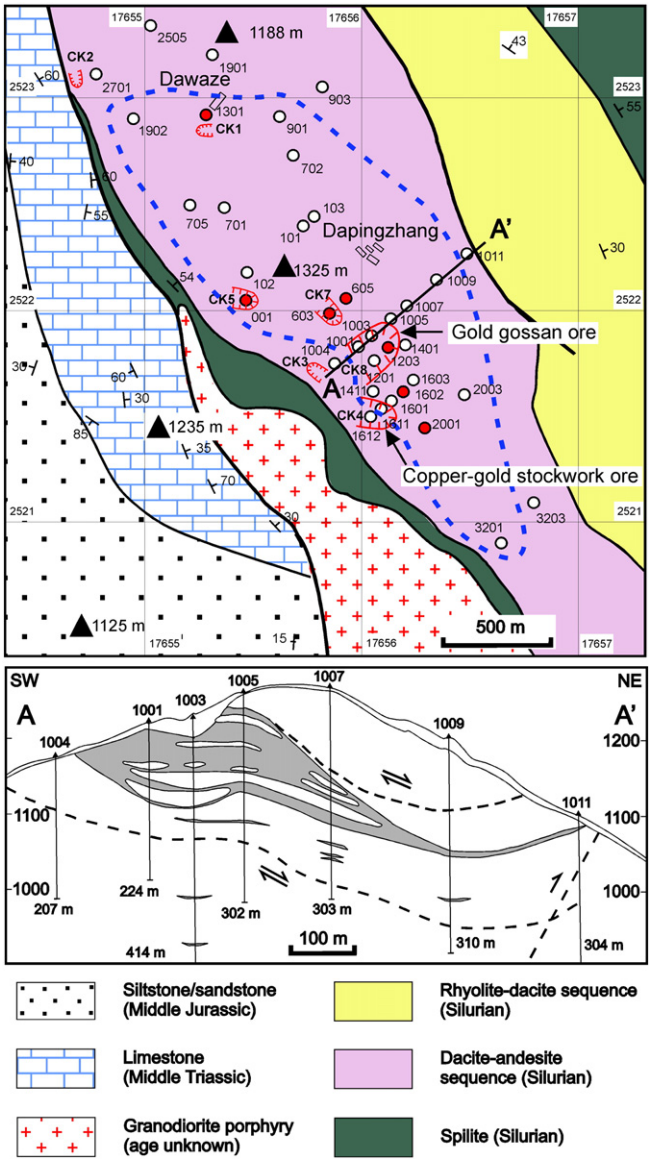

Fig. 3. Local geology of the Dapingzhang volcanic-hosted massive sulfide and stockwork ore deposit. The plan view shows the outline of the orebody (stippled line) of mostly stockwork ore according to drill data (circles). Outcrops/open pits with massive sulfide mineralization are numbered CK1 to CK8, drill holes that encountered disrupted massive sulfide lenses are shown in red circles. The cross-section A–A′ shows the sheared stockwork orebody (0.3% Cu cut-off) in gray shading, which includes both massive sulfide ore and stockwork ore (dominant). Samples for Re–Os dating are from drill holes 603, 605, 1602, and 1611, all in the central part of the orebody.

basin. The basement of this basin is only exposed near its margins and in a few fault-bounded anticlines or horst structures. The Dapingzhang deposit is located in the core of such an anticline/horst (Fig. 2). The tectonic windows represented by the Dapingzhang anticline, the Yunxian anticline 15 km to the east, and the Yinzishan anticline 25 km to the south, expose a volcaniclastic sequence possibly >2000 m in thickness (Yang et al., 2000), with spilite in the lower part, overlain by dacite–andesite lava and tuff, rhyolite, siltstone, and chert.

Strongly sheared polymetallic massive sulfide mineralization, dominated by pyrite–chalcopyrite–sphalerite–galena, and an associated pyrite–chalcopyrite stockwork zone are located in the lowermost dacite–andesite sequence at the Dapingzhang deposit (Fig. 3). Both Late Devonian and Early Carboniferous radiolaria were described from chert lenses on top of the massive sulfide orebody at Dapingzhang (Feng et al., 2000). However, Feng et al. (2000, 2002) also note that the rocks in these tectonic windows are distributed in thrust slices, and stratigraphic contact relations are disturbed. A complex sedimentary sequence from the Late Carboniferous to Middle Triassic, which includes blocks of Early Devonian carbonate rocks and several angular unconformities, has been described from the Yunxian anticline based on conodonts and radiolarians (Feng et al., 2002, 2005).

The volcaniclastic series at Dapingzhang is discordantly overlain by Middle Triassic clastic rocks and massive limestone, which is in turn unconformably overlain by Jurassic continental siltstone/sandstone with a basal polymict conglomerate, including pebbles of Triassic limestone. The Jurassic red bed sequence, with its well developed basal conglomerate, is a typical unit throughout the Simao basin. It also outcrops west of the Lancang River, where the Jurassic cover unconformably overlies both the Triassic Lincang granite and the surrounding Proterozoic mica-schist.

4. Samples and methods

4.1. Major and trace element analysis

Sixty representative bulk-rock and ore samples from the 8000 m of drillcore, obtained during the Dapingzhang exploration project in 1999–2001, were selected during field work in 2003. Additional grab samples were taken from the open pit from 2006 to 2009. Representative parts of the 1–2 kg samples were prepared for microscopic/electron microprobe work on polished thin sections. The majority of the samples were crushed and powderized in an agate shatter box. Major elements and a number of trace elements were analyzed by X-ray fluorescence (XRF) spectrometry on lithium metaborate fused disks at Federal Institute for Geosciences and Natural Resources (BGR), Hannover, Germany. Relative uncertainties of the XRF analyses are ≤3% for major elements and 10–20% for most trace elements. The REEs and most trace elements were analyzed by a combination of instrumental neutron activation (INA) analysis, inductively-coupled plasma (ICP) analysis, and inductively-coupled plasma and mass spectrometry (ICP-MS) analysis, with a three-acid digestion (HF–HCl–HNO_3) used for ICP and ICP-MS analysis by Activation Laboratories Ltd. in Ancaster, Ontario, Canada. Relative uncertainties are similar to the trace element program of XRF analysis. The full data set is documented in ESM Tables 1 and 2. Data on ten representative samples from the whole data set of more than 60 samples are shown in Tables 1a and 1b.

4.2. Nd isotope analysis

Samarium–Nd isotope analysis of whole-rock powders (Table 1c) was performed at the Federal Institute for Geosciences and Natural Resources (BGR) in Hannover, Germany. The Sm and Nd element fractions obtained by standard separation techniques were loaded on Re filaments and run on a double-filament assembly in static mode using a ThermoFinnigan TRITON mass spectrometer equipped with nine Faraday collectors. Element concentrations were determined by isotope-dilution techniques. Isotopic ratios were normalized to $^{146}Nd/^{144}Nd = 0.7219$ for Nd and to $^{154}Sm/^{149}Sm = 1.64609$ for Sm. Procedural blanks are less than 0.1% of the relevant sample concentration and are therefore negligible. A Nd element standard (Merck™) run routinely in the course of the sample measurements yielded $^{143}Nd/^{144}Nd = 0.512395 \pm 0.000007$ (2SD; n = 10), which corresponds to $^{143}Nd/^{144}Nd = 0.511845$ for the LaJolla Nd standard (cross-calibrated at the BGR). Uncertainties at the 95% confidence level are 0.0025% for $^{143}Nd/^{144}Nd$, and 1% for $^{147}Sm/^{144}Nd$, respectively. Calculation of the Sm–Nd model parameter ε_{Nd} is based on $^{143}Nd/^{144}Nd = 0.512638$ and $^{147}Sm/^{144}Nd = 0.1967$ for a CHUR reference ('chondritic uniform reservoir'; Jacobsen and Wasserburg, 1980). Single-stage depleted-mantle model ages (T_{DM}) were calculated

Table 1a
Representative major and trace element data for Dapingzhang and Yinzishan.

Sample rock type	SiO_2	TiO_2	Al_2O_3	ΣFe_2O_3	MnO	MgO	CaO	Na_2O	K_2O	P_2O_5	(SO_3)	LOI	Sum
	wt.%	wt.%	wt.%	wt.%	wt.%	wt.%	wt.%	wt.%	wt.%	wt.%	wt.%	wt.%	wt.%
	XRF	XRF	XRF	XRF	XRF	XRF	XRF	XRF	XRF	XRF	XRF	Grav	
Dapingzhang													
2701/2 Dacite	67.08	0.806	14.59	5.30	0.052	1.06	0.81	5.38	1.24	0.056	0.24	3.18	99.72
3201/2 Dacite	72.93	0.208	12.62	2.37	0.097	0.84	2.16	3.58	1.73	0.038	0.26	2.95	99.75
3203/2 Dacite	74.24	0.317	12.52	2.46	0.037	0.55	1.50	4.90	0.97	0.066	0.25	1.93	99.76
D 35 Granite porphyry	75.18	0.188	12.59	2.40	0.068	0.36	0.47	5.51	1.06	0.038	0.02	1.83	99.70
D-36 Meta-basalt (spilite)	45.57	0.828	16.06	12.75	0.236	5.58	5.84	4.47	0.13	0.102	0.29	7.97	99.60
D-42 Dacite	67.40	0.342	12.74	1.98	0.037	9.35	0.20	1.93	0.17	0.070	0.26	5.37	99.76
D-46 Dacite	88.16	0.035	6.88	0.24	0.006	0.07	0.06	3.37	0.12	0.016	<0.01	1.00	99.85
Yinzishan													
D 8 Andesite	55.09	0.415	13.75	7.94	0.189	3.44	6.20	5.09	0.50	0.062	2.43	4.59	99.72
Lancangjiang valley													
S 5 Lincang granite	67.74	0.643	14.06	4.79	0.080	2.48	2.84	2.49	3.628	0.181	0.04	0.55	99.55
S 6 Tertiary microgranite	76.57	0.060	12.58	1.17	0.049	0.09	0.60	3.13	4.889	0.014	0.09	0.53	99.79

Sample rock type	As	Ba	Bi	Co	Cr	Cs	Cu	Ga	Hf	Mo	Nb	Ni	Pb
	ppm	ppm	ppm	ppm	ppm	ppm	ppm	ppm	ppm	ppm	ppm	ppm	ppm
	INA	XRF	ICPMS	ICPMS	XRF	ICPMS	ICPMS	ICPMS	ICPMS	INA	ICPMS	ICPMS	ICPMS
Dapingzhang													
2701/2 Dacite	20	168	0.21	12.8	10	4.39	4.9	16.3	3.4	<1	6.7	8.7	7.1
3201/2 Dacite	4.7	271	0.04	4.0	<3	2.59	5.5	11.3	2.1	<1	2.3	3.5	1.8
3203/2 Dacite	4.1	220	0.03	2.4	<3	1.08	5.0	13.1	2.3	4	2.3	5.5	2.2
D 35 Granite porphyry	5.4	237		3.0	<3	<1	7.0	11.0	3.0	1	<2	1.0	<2
D-36 Meta-basalt (spilite)	2.8	57	0.08	41.9	11	0.29	11.3	19.5	1.1	<1	1.2	794	2.3
D-42 Dacite	2.4	59	0.09	1.1	<3	0.94	314	16.0	3.1	3	2.7	4.2	7.5
D-46 Dacite	15.4	56	0.13	0.3	<3	0.29	7.5	4.2	1.6	<1	3.0	5.1	2.8
Yinzishan													
D 8 Andesite	41.9	280	0.20	28.0	32	0.40	122	16.6	1.4	<1	1.7	23.8	30.7
Lancangjiang valley													
S 5 Lincang granite	0.5	883	0.39	13.7	105	8.79	19.1	18.9	0.6	15	14.7	47.5	33.8
S 6 Tertiary microgranite	<0.5	378	0.18	1.5	32	9.33	25.5	13.1	2.9	<1	6.9	26.0	43.6

Sample rock type	Rb	Sb	Sc	Sn	Sr	Ta	Th	U	V	W	Zn	Zr
	ppm	ppm	ppm	ppm	ppm	ppm	ppm	ppm	ppm	ppm	ppm	ppm
	ICPMS	INA	INA	XRF	ICPMS	ICPMS	ICPMS	INA	ICP	INA	XRF	XRF
Dapingzhang												
2701/2 Dacite	13.8	1.2	14.9	3	298	0.5	2.4	<0.5	117	<1	72	115
3201/2 Dacite	13.1	<0.1	7.8	<2	60.0	0.1	3.0	3.1	33	3	49	67
3203/2 Dacite	6.3	0.5	19.5	<2	97.1	0.1	2.0	4.8	12	<1	95	52
D 35 Granite porphyry	16.0	0.3	11.6	3	94.0	<0.5	3.7	1.1	<5	<1	51	117
D-36 Meta-basalt (spilite)	0.7	<0.1	42.6	<2	145	<0.1	0.7	<0.5	357	<1	114	24
D-42 Dacite	2.3	<0.1	18.6	<2	58.8	0.2	2.4	2.6	21	<1	415	53
D-46 Dacite	2.8	4.2	4.4	<2	40.7	0.1	3.9	1.5	<2	<1	14	49
Yinzishan												
D 8 Andesite	5.3	<0.1	33.1	2	72.5	0.1	1.6	<0.5	216	<1	145	39
Lancangjiang valley												
S 5 Lincang granite	137	0.7	14.6	3	197	1.5	21.4	8.8	91	<1	117	208
S 6 Tertiary microgranite	207	1.1	2.8	<2	59.4	0.9	22.0	12.5	3	<1	14	83

assuming $^{143}Nd/^{144}Nd = 0.513151$ and $^{147}Sm/^{144}Nd = 0.219$ for the present-day depleted-mantle reservoir and a linear isotope evolution through time. In all calculations, the IUGS-recommended constants (Steiger and Jäger, 1977) were used.

4.3. Re–Os isotope analysis

Eight bulk rock samples from drill core were selected for Re–Os isotope analysis based on multielement geochemical data. The chosen samples were characterized by elevated and correlated Mo and Re contents in the range of 35–629 ppm Mo (INA data) and 55–152 ppb Re (ICP-MS data), respectively (ESM Table 2). The Re–Os isotope analyses were made in the Low blank Re–Os lab, National Research Center of Geoanalysis, Chinese Academy of Geological Sciences, Beijing. The enriched ^{190}Os and enriched ^{185}Re were obtained from the Oak Ridge National Laboratory. A Carius tube digestion was used (Shirey and Walker, 1995; Du et al., 2004).

The ICP-MS measurement was performed with a TJA PQ ExCELL ICP mass spectrometer. The instrument was optimized to $>5\times10^4$ cps for 1 ng/mL ^{115}In and $>5\times10^4$ cps for 1 ng/mL ^{238}U. Data acquisition was in peak-jumping mode with a dwell time of 15 ms. The isotopes for Re measurement are ^{185}Re and ^{187}Re. The ^{190}Os is selected as the

Table 1b
Representative REE data for Dapingzhang and Yinzishan.

Sample rock type	La	Ce	Pr	Nd	Sm	Eu	Gd	Tb	Dy	Y	Ho	Er	Tm	Yb	Lu
	ppm	ppm	ppm	ppm	ppm	ppm	ppm	ppm	ppm	ppm	ppm	ppm	ppm	ppm	ppm
2701/2 Dacite	12.2	29.7	3.13	12.9	3.22	0.88	3.06	0.46	2.73	10.7	0.55	1.75	0.25	1.87	0.30
3201/2 Dacite	9.5	22.2	2.35	8.47	2.03	0.62	2.17	0.33	1.92	9.22	0.41	1.25	0.19	1.43	0.20
3203/2 Dacite	13.3	30.8	3.91	17.8	4.72	1.31	4.92	0.71	4.07	23.1	0.89	2.91	0.47	3.66	0.57
D35 Granite porphyry	10.5	20.0		6.00	2.70	0.80		<0.5		22.0				4.20	0.63
D36 Meta-basalt (spilite)	2.9	7.17	1.01	4.79	1.47	0.53	1.69	0.29	1.83	8.49	0.39	1.27	0.17	1.30	0.19
D42 Dacite	11.1	12.4	3.45	16.2	4.84	1.38	5.74	0.97	6.32	32.5	1.32	4.13	0.63	4.25	0.64
D46 Dacite	10.5	23.2	3.12	12.60	3.43	0.24	4.12	0.76	5.68	36.4	1.35	4.44	0.69	4.95	0.77
Yinzishan															
D8 Andesite	3.3	7.14	0.97	4.52	1.42	0.41	1.93	0.35	2.49	15.4	0.55	1.79	0.27	1.76	0.27
Lancangjiang valley															
S5 Lincang granite	46.1	93.0	10.5	39.4	8.33	1.15	7.05	1.00	5.57	22.8	1.02	2.66	0.39	2.51	0.31
S6 Tertiary microgranite	28.7	57.3	5.61	19.2	3.65	0.41	3.02	0.45	2.90	15.4	0.58	1.97	0.30	2.21	0.31

monitor for ^{187}Os contamination. The selected isotopes for Os measurement are ^{187}Os, ^{190}Os, and ^{192}Os. The ^{185}Re is selected as the monitor for ^{187}Re contamination in the ion-exchange solution. The average blanks for the total Carius tube procedure are about 2 pg Re and 0.85 pg Os.

4.4. U–Pb zircon analysis

We collected two large bulk-rock dacite samples (20 kg), one from the Dapingzhang open pit and a second from an outcrop along the Simao–Simao Gang highway, about 1 km east of the Yinzishan mine (22°35′9.9″, 100°35′48.8″) (Fig. 2). The open pit sample proved to have such a high degree of pervasive quartz–sericite overprint that no magmatic zircons could be separated. However, the second sample, which was less altered, yielded a large amount of magmatic zircons of idiomorphic shape that were separated using shaking table and heavy liquid techniques (ESM, Fig. 1). These zircons were analyzed using a Geolas 193 nm ArF Excimer laser ablation (LA) system equipped with an Agilent 7700× ICP-MS, at the Institute of Geochemistry, Chinese Academy of Sciences, Guiyang, China. Ablation time was about 45 s for 225 pulses of each measurement, with a 5 Hz repetition rate on a stationary spot of ~32 μm. Helium was the carrier gas. Harvard zircon 91500 and NIST 610 glass were used as the external standards to normalize isotopic discrimination and element concentrations, respectively. Standard zircons GJ-1 and PL were tested for quality control. Data reduction was performed off-line by *ICPMSDataCal* (Liu et al., 2010) and then processed using the ISOPLOT program of Ludwig (2009) (Table 3).

5. Petrography and geochemistry of the volcaniclastic dacite–andesite sequence and tectonomagmatic characterization

The volcaniclastic host sequence for the Dapingzhang VHMS deposit texturally consists of very heterogeneous and brecciated volcanic rocks, with mostly strong hydrothermal overprint. The dacite–andesite has a distinct banded or flaser-like texture resulting from parallel arrangement of dark greenish-gray lenticular and irregular shard-like domains, which are mm- to cm-size and consisting of chlorite–sericite or clay, hosted in a dense light-gray quartz–chlorite–clay groundmass. This eutexitic texture is similar to that of welded tuffs and suggests former glass fragments that have been compacted into parallel disk-shaped lenses, but could also result from clay-rich sediment fragments in dacite–andesite tuff. The rock contains 5–20% corroded cataclastic quartz phenocrysts, relics of feldspar phenocrysts that are clay or sericitic altered, and/or clay–chlorite–altered/sericitized xenolithic/autolithic rock fragments set in a very-fine grained granoblastic quartz–chlorite/sericite–clay matrix with disseminated pyrite. Quartz is abundant as veinlets and in patchy mosaics in the groundmass. Some rock samples have a more homogeneous lava-like porphyritic fabric with corroded quartz, plagioclase, and K-feldspar crystals set in a very fine-grained matrix.

The lower spilite unit of the volcaniclastic sequence consists of a dense green rock with small sub-mm sized rounded vesicules filled by carbonate and rimmed by chlorite. The rock has a relict intersertal fabric composed of sparsely distributed idiomorphic and carbonatized feldspar phenocrysts set in a groundmass of very fine-grained albite laths and chlorite (Fig. 4). Chlorite–carbonate alteration is very pronounced,

Table 1c
Samarium–neodymium concentration and isotope data.
All constants for calculation of ε_{Nd} and T_{DM} from Faure (1986).

Sample	Rock type	Age (Ma)	Sm (ppm)	Nd (ppm)	$^{147}Sm/^{144}Nd$	$^{143}Nd/^{144}Nd$	$\varepsilon_{Nd}(t)$	T_{DM}
Dapingzhang								
3203/2	Dacite	429	4.72	18.32	0.1559	0.512731	4.1	883
D46	Dacite	429	3.29	12.09	0.1643	0.512781	4.6	880
D42	Dacite	429	4.11	14.25	0.1744	0.512776	3.9	1082
2701/2	Dacite	429	4.12	19.41	0.1282	0.512572	2.5	881
3201/2	Dacite	429	2.07	9.57	0.1307	0.512714	5.1	668
D36	Basalt (spilite)	429	1.34	4.64	0.1741	0.512851	5.4	837
D8	Basalt (spilite)	429	1.17	3.82	0.1857	0.512550	−1.1	2357
D35	Granite porphyry	(340)	3.73	13.76	0.1638	0.512806	4.7	807
Lancang river area								
S6	Microgranite	40	4.47	24.24	0.1114	0.512406	−4.1	976
S5	Lincang granite	240	8.51	43.70	0.1177	0.511950	−11.0	1697

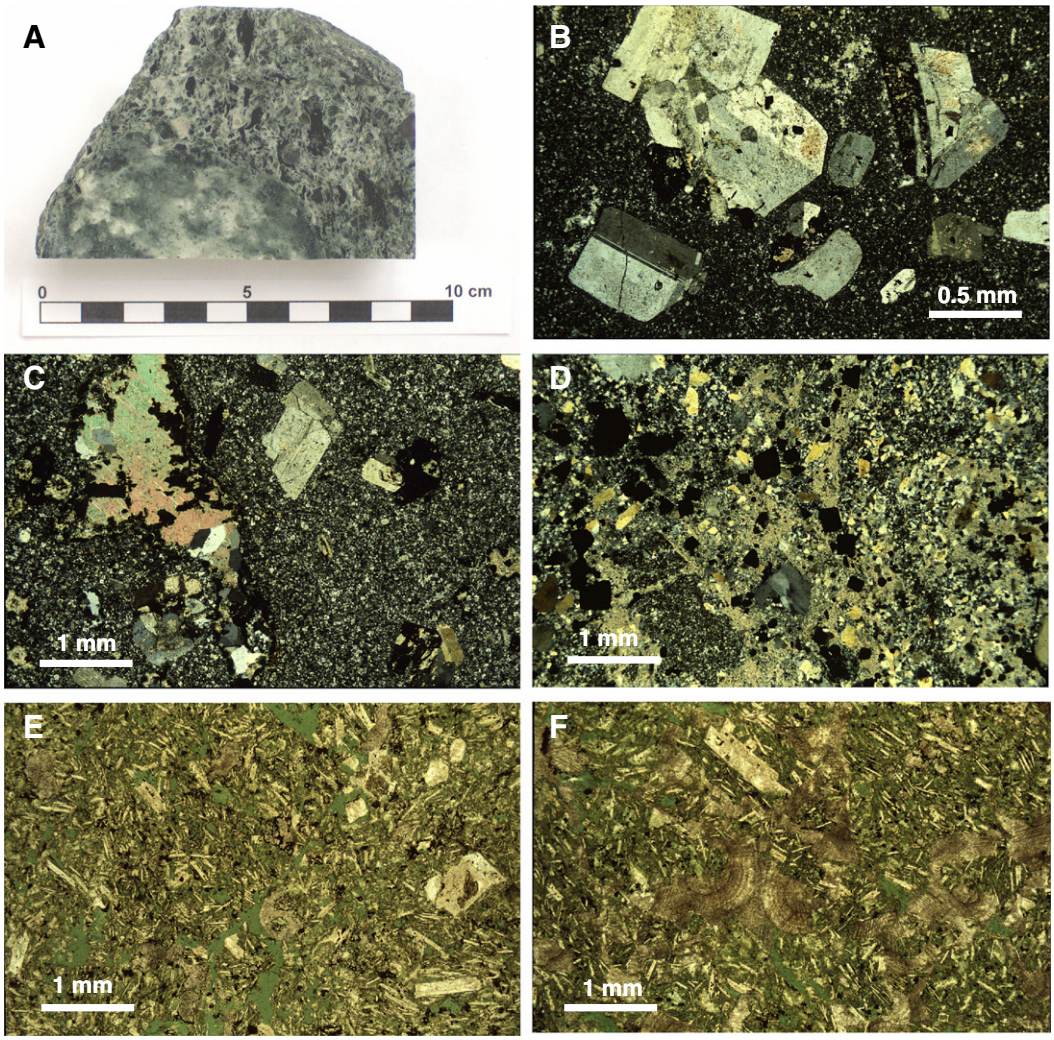

Fig. 4. Petrography of the dacite–andesite and spilite sequence. A. Typical welded (?) texture of dacite with irregular/lenticular dark green domains, probably former glass shards that are now chlorite–clay, and autolithic inclusion of milky appearance that is a strongly silicified tuff. Pervasive propylitic alteration and silicification are present. Drill core 3201/1, 85 m. B. Dacite porphyry. Transmitted light (+), drill core 3203/2, 120 m. C. Dacite with propylitic alteration (carbonate–chlorite–pyrite–titanite). Transmitted light (+), drill core 103/2, 147 m. D. Dacite breccia/quartz–pyrite stockwork with phyllic alteration (quartz–illite/sericite–pyrite). Transmitted light (+), drill core 605/8, 126 m. E. Spilite (metabasalt) with propylitic alteration consisting of albite–chlorite–dolomite. Transmitted light (//), surface D36, Dapingzhang South. F. Spilite (metabasalt) with propylitic alteration consisting of albite–chlorite–dolomite with advanced dolomite blastesis in concentric aggregates. Transmitted light (//), surface DAP 1, Yinzishan mine.

with larger granoblastic patches of chlorite and carbonate. Advanced carbonate blastesis, locally characterizing as much as 50% of the rock volume, is expressed as rounded and concentrically zoned, sub-mm to cm-size carbonate aggregates and as carbonate veinlets that extinguish the primary intersertal rock fabric (Fig. 4). Epidote–clinozoisite, quartz, and opaque minerals are abundant on sheared veinlets and in granoblastic aggregates.

The chemical composition of the volcanic sequence ranges mainly from dacite to andesite, with minor units of rhyolitic and basaltic composition (Fig. 5). Sodium and Ca are mostly strongly leached (<0.1 wt.% Na_2O, <0.2 wt.% CaO), but enriched in some spilite samples (basalt transformed into chlorite–albite–carbonate rock). Calcium and Mg are also locally enriched in stockwork ore producing dolomite. Magnesium shows an erratic distribution with values as large as 13 wt.% MgO in some stockwork ore samples where magnesium is fixed in chlorite.

A characteristic feature of the dacite–andesite sequence is its low abundance of Nb, Ta, Zr, Th, Ti, and REE. These elements allow a discrimination of the tectonomagmatic environment, particularly a distinction between arc and non-arc environments (Briqueu et al., 1984). Subduction settings are characterized by a relative depletion in Nb and Ta and enrichment in Th with respect to REE of similar chemical character. All samples of the dacite sequence have distinctive negative Nb–Ta anomalies and Th enrichment when normalized to chondrite/primitive mantle (Fig. 6). They also have Nb/Th ratios consistently <2, which is a diagnostic feature of arc environments (Swinden, 1996). This also applies to the most mafic members of the volcanic rock sequence, i.e. the metabasaltic spilite rocks that can be assumed to be derived from magmas least affected by continental crust contamination.

The multielement distribution pattern of the dacite–andesite sequence at Dapingzhang is much different from the Permo-Triassic rhyolite–alkali basalt sequence a few kilometers west. At the latter, little or no subduction component is visible, because there is no Ta trough and Nb/Th ratios are as great as 12. The origin of these basalts is continental rift- or plume-related (Heppe, 2006). The Dapingzhang rocks have ε_{Nd} (t = 429 Ma; see below) values of +2 to +5, omitting one spilite sample with a value of −1.1, and have a Nd isotope composition similar to the Permo-Triassic alkali basalt (Heppe, 2006). Therefore, they are also mainly derived from the mantle or young continental crust.

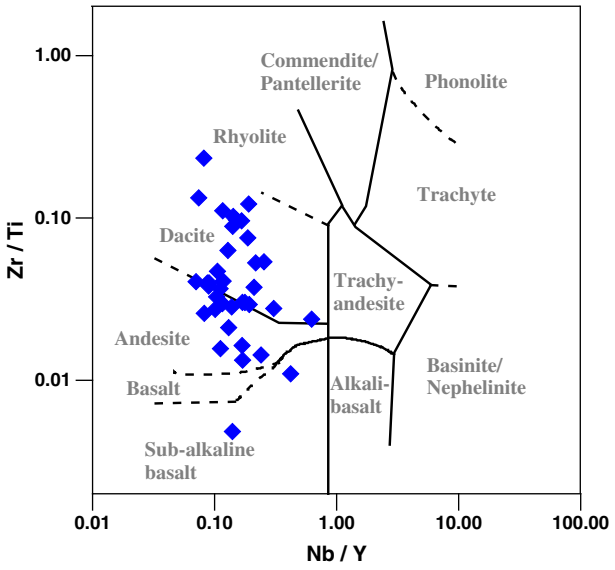

Fig. 5. Bulk-rock compositions of the Dapingzhang volcaniclastic sequence in a Zr/Ti versus Nb/Y.
After Winchester and Floyd (1977).

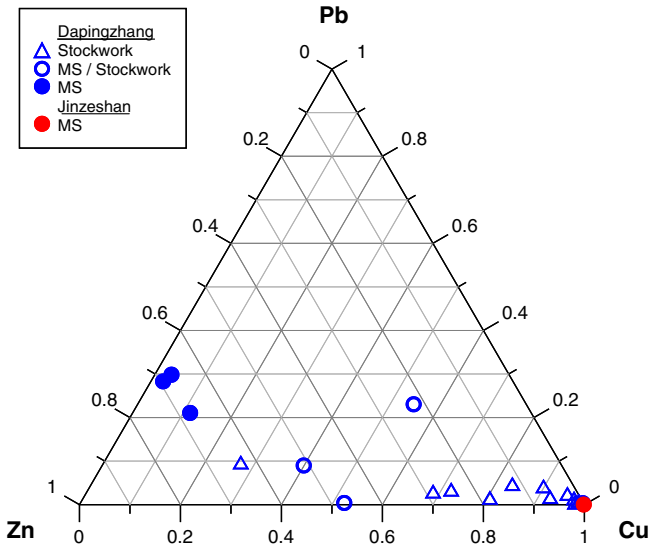

Fig. 7. Ore samples in a Pb–Cu–Zn triangle plot. The massive sulfide ore from Dapingzhang plots mostly in the Zn–Pb–Cu group of Franklin (1996), while the stockwork ore is dominated by Cu.

6. Mineralization style and ore petrography of the Dapingzhang deposit

The Dapingzhang VHMS deposit was discovered by local farmers in 1996 and was then explored by the No. 5 Geological Brigade of the Yunnan Bureau of Geology and Mineral Resources. The deposit was initially artisanally mined for its gold-rich gossan, and has been mined at larger scale by the Yunnan Simao Shansui Copper Company since 2006.

The Dapingzhang deposit has two styles of mineralization. First, polymetallic massive sulfide ore is present as disrupted 1- to 6-m-thick, flat-lying sulfide lenses. The estimated resource of this ore is 1.8 million tonnes (Mt) at 3.8% Cu, 2.3% Pb, 7.0% Zn, 2.9 g/t Au, and 145 g/t Ag. Second, copper stockwork ore within a NW-trending area of 2600×100–800 m, concentrated within disrupted domains that are as much as 40-m-thick, contains 45 Mt at 1.1% Cu, 0.3% Pb + Zn, 0.2 g/t Au, and 5 g/t Ag, with a cut-off at 0.3% Cu. A gold-rich gossan, present as a 1- to 2-m-thick blanket of iron oxide/hydroxide with about 3 g/t Au, was selectively mined by artisanal cyanide-heap leaching in the central part of the ore deposit before large-scale open-pit mining started. The metallogeny of the deposit places the ore in the non-auriferous (or "ordinary") group of VHMS deposits at the transition of the copper–zinc to the zinc–lead–copper group (Fig. 7) (Franklin, 1996; Mercier-Langevin et al., 2011).

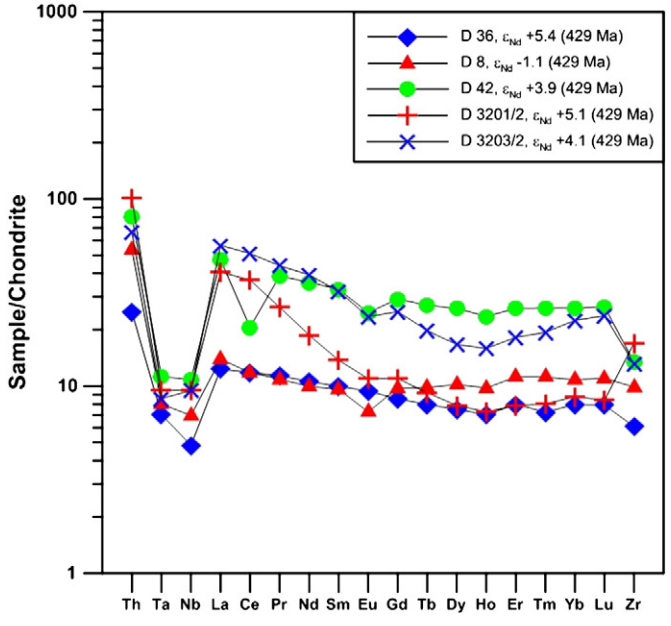

Fig. 6. Multielement plot for rock samples from the dacite–andesite sequence of the Dapingzhang area. Sample D 36 is spilite (metabasalt), the other samples are dacite–andesite. Sample D 8 is spilite from the Yinzishan satellite massive sulfide occurrence, about 20 km SSW of Dapingzhang. Note the distinctive Nb–Ta anomaly typical of subduction-related rocks. Initial Nd isotope data indicate a dominantly mantle origin with little contamination by old continental crust.

A particularly significant feature of the Dapingzhang deposit is that most of the resource is hosted in a stockwork system that is as much as 40-m-thick. The spatial relationship to the massive sulfide ore is commonly tectonically disturbed. However, the main pit zone, which is also the center of the deposit, exposes sheared massive sulfide material on top of a thick stockwork zone. Massive sulfide ore in drill holes is, however, not underlain by stockwork mineralization. This lack of consistent spatial association is probably due to the extreme difference in mechanical behavior of the two ore styles during shear deformation, such that the incompetent massive sulfides are more easily ductilely deformed relative to the competent silicified dacite/quartz–sulfide stockwork.

The dacite–andesite sequence with spilite is also exposed in a small anticlinal structure about 25 km SSE of Dapingzhang at the artisanal Yinzishan (Silver Mountain) underground mine (Fig. 2). Massive sulfide mineralization, composed of pyrite–hematite–chalcopyrite–sphalerite and as much as 15-cm-thick, occurs here in a shear zone and could represent similar VHMS mineralization. Hematitization is very distinct and the ore grade is about 2% Cu, 1–6 g/t Au and 200 g/t Ag. Outcrops of the dacite sequence in the area display strong propylitic alteration and argillic alteration.

The textural diversity of the Dapingzhang ore is portrayed in Fig. 8. Ore mineralogy and texture of the VHMS ore are different in the northwestern and southeastern part of the deposit. The ore is granoblastic in the southeastern part and is dominated by pyrite (60–90%), with the remainder consisting of chalcopyrite (5–20%), sphalerite (5–20%), and galena (<5%). There is a hydrothermal overprint of the massive ore and an extensive underlying quartz–pyrite–chalcopyrite stockwork (feeder zone). The northwestern part of the deposit, termed the Dawaze section, has sedimentary textures that are well preserved and much more sphalerite (≤30%) and galena

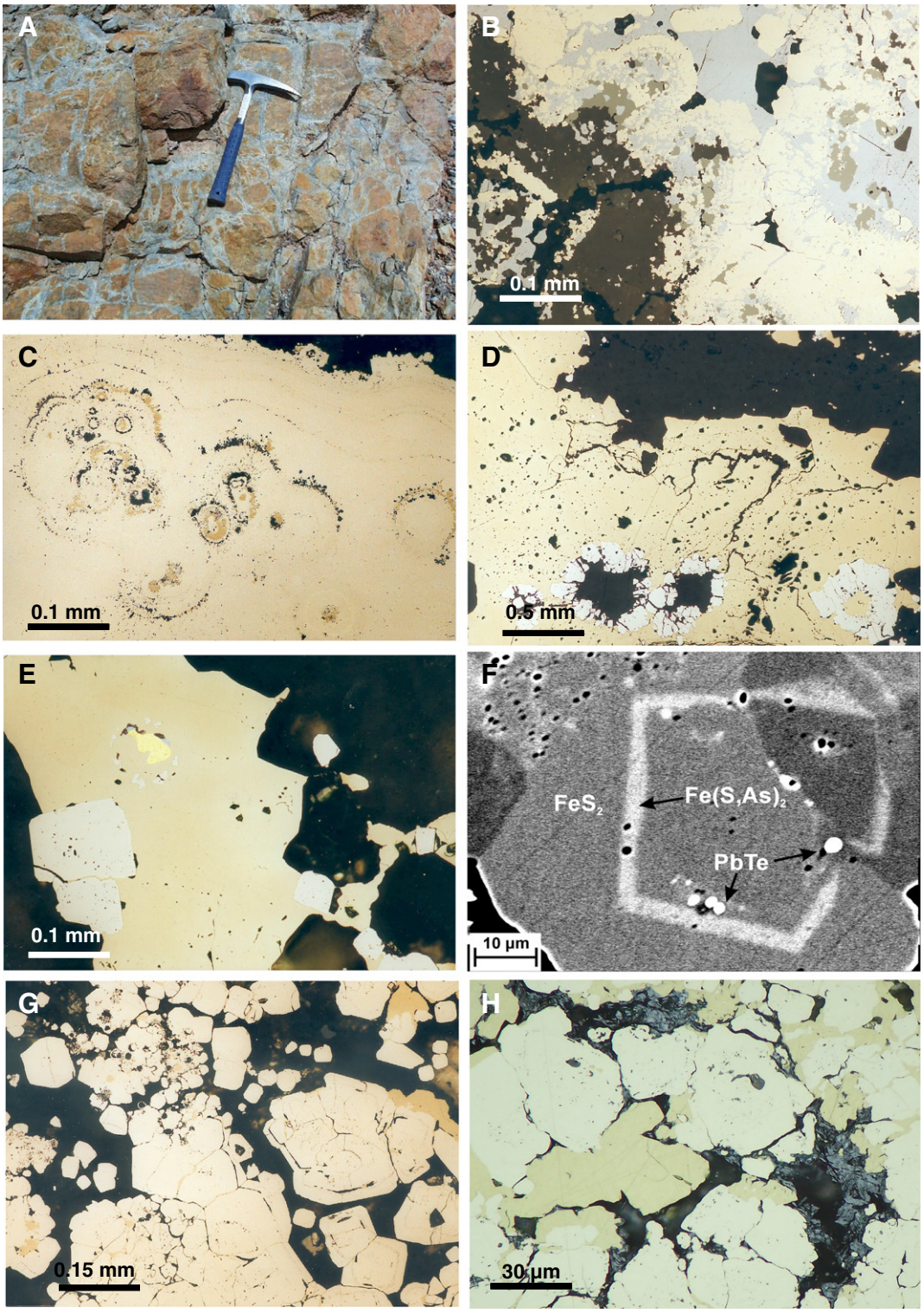

Fig. 8. Ore petrography. A. Copper stockwork ore with oxidized copper-rich sulfide veinlets in quartz–sericite altered dacite. Dapingzhang main pit (CK 4). B. Polymetallic massive sulfide ore: pyrite with colloform structure, galena, tetrahedrite (olive-gray; in galena), sphalerite (dark gray), barite (black). Reflected light, oil immersion, Dawaze section D5. C. Polymetallic massive sulfide ore: pyrite–chalcopyrite with colloform structure. Reflected light, oil immersion, Dapingzhang main pit D7. D. Stockwork ore: pyrite in atoll structure (gel relics?) in chalcopyrite, quartz (black). Reflected light, air, Dapingzhang main pit D17. E. Stockwork ore: gold (17 wt.% Ag) with corona of galena inclusions in chalcopyrite, idiomorphic pyrite, quartz. Reflected light, oil immersion, Dapingzhang main pit D17. F. Massive sulfide/stockwork ore (transition zone): As zoning in pyrite (0–2.9 wt.% As) and altaite inclusions. Back-scattered electron image, drill core 1007/2, 127 m. G. Massive sulfide/stockwork ore (transition zone): zoned pyrite idioblasts and framboids, chalcopyrite, quartz (black). Reflected light, oil immersion, drill core 603/1, 14 m. H. Stockwork ore: molybdenite intergrown with quartz, interstitial to pyrite–chalcopyrite porhyroblasts. Reflected light, oil immersion, drill core 603/1, 14 m.

(≤20%), as well as tennantite–tetrahedrite (≤5%). Barite is locally abundant (≤50%). Ore texture and mineralogy in the northern part document a vent distal position.

The copper stockwork ore mainly consists of quartz, pyrite, and chalcopyrite, with minor amounts of sphalerite and galena. Pyrite is commonly idioblastic, locally chemically zoned with as much as

3 wt.% As, and, in places, shows unusual zonal intergrowth with galena. There are various stages of recrystallization of pyrite, with formation of atoll structures from colloform pyrite aggregates (Fig. 8), similar to that described from the Kuroko-style VHMS deposits in Japan (Yui, 1983). Incipient recrystallization of colloform pyrite is also observed in the non-metamorphosed parts of the Kuroko ore (Eldridge et al., 1983) and in the Devonian Rammelsberg sedimentary rock-hosted massive sulfide deposit, Germany (Kraume, 1955). Pyrite contains abundant Te–Bi-bearing mineral inclusions in the μm size range. Sphalerite forms mostly small inclusions in pyrite

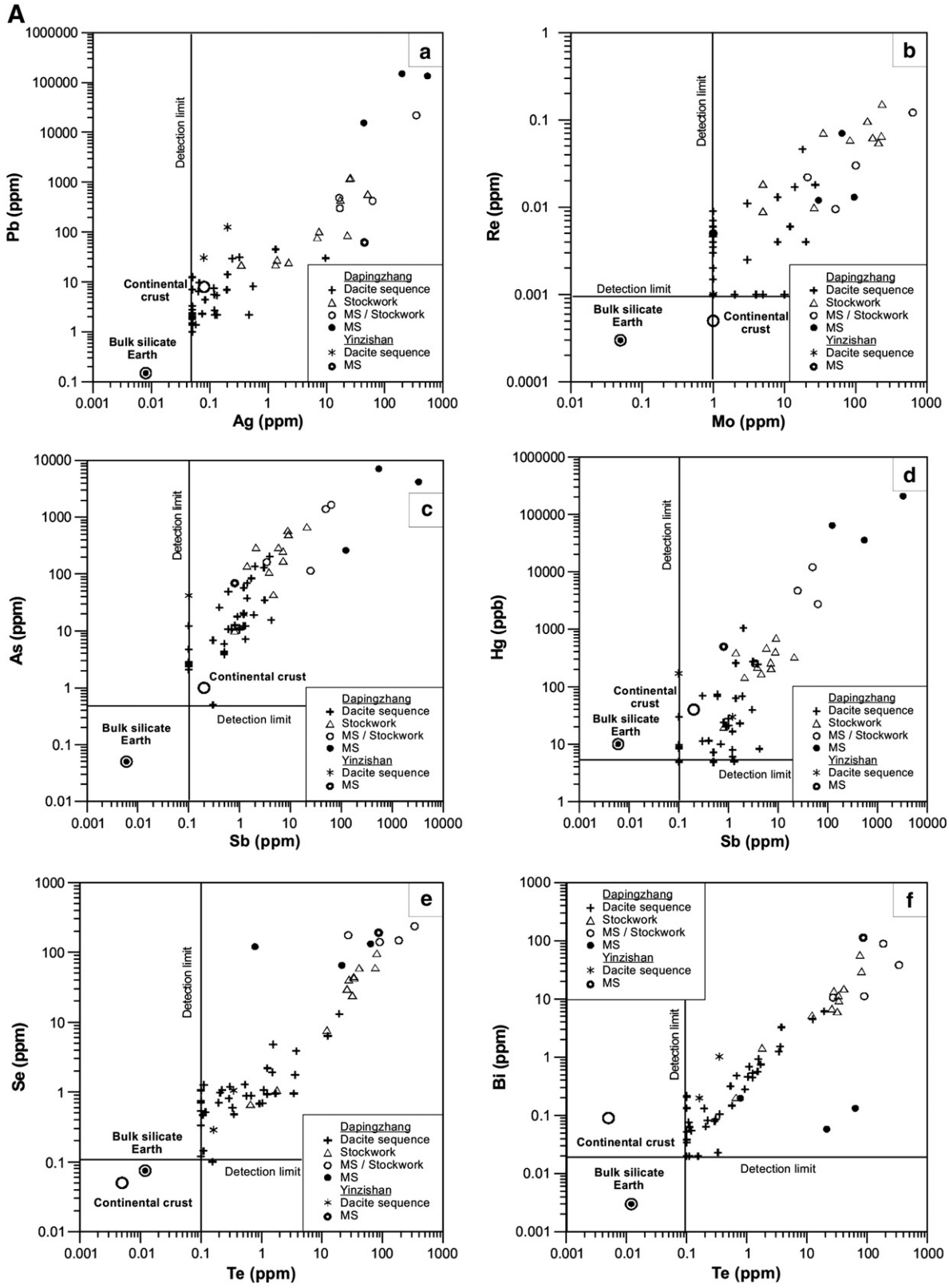

Fig. 9. a. Variation diagrams for bulk rock and ore samples from the Dapingzhang and the satellite Yinzishan deposits. MS = Massive sulfide ore. b. Gold versus Ag, Cu, As, Se, Te, and Bi variation diagrams for bulk rock and ore samples from the Dapingzhang and the satellite Yinzishan deposits. MS = Massive sulfide ore.

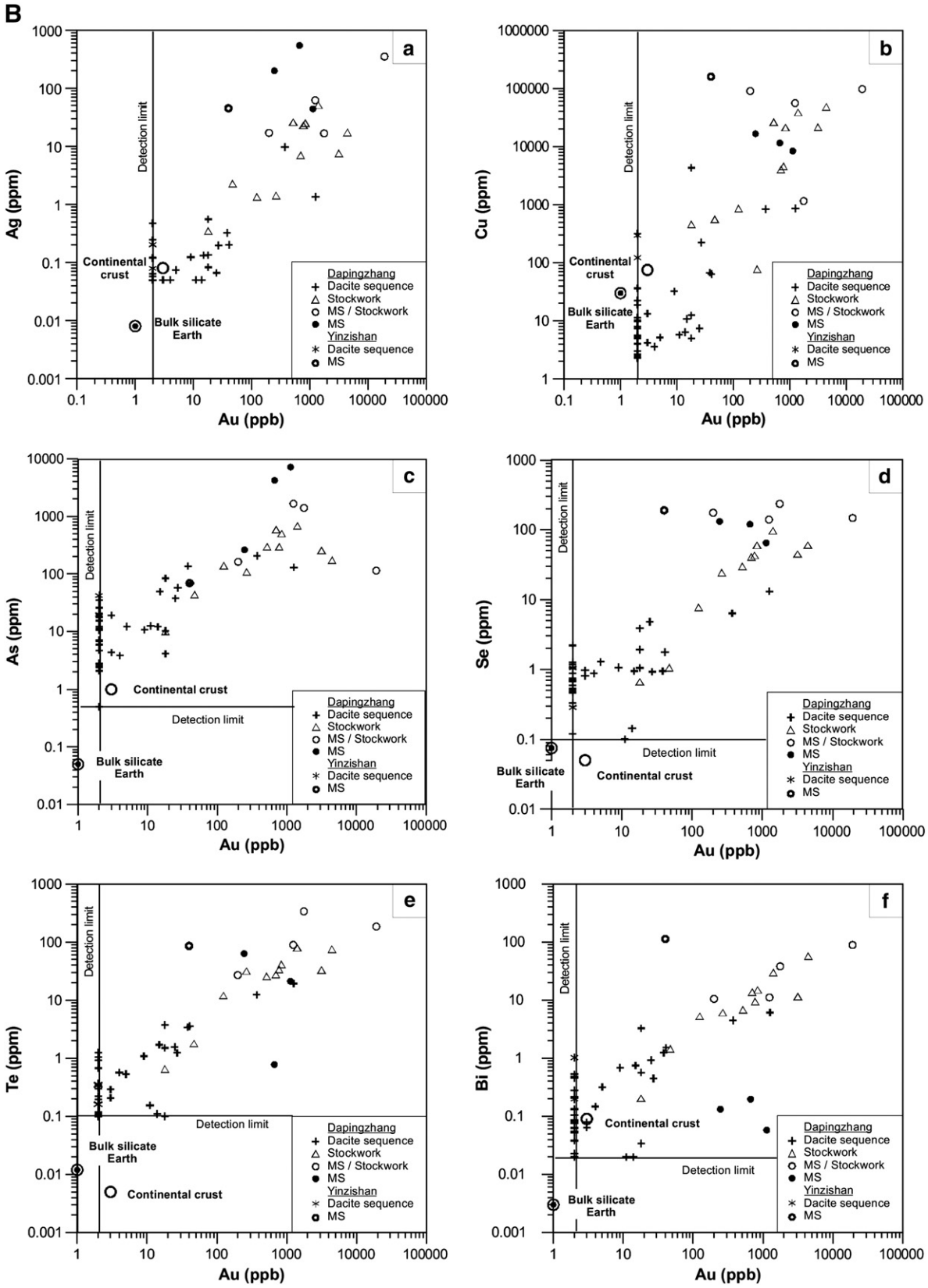

Fig. 9 (*continued*).

and chalcopyrite and has as much as 5 wt.% Fe and 0.6 wt.% Cd. Incipient alteration to covellite is frequent along grain boundaries. Galena commonly has <1 wt.% Se and ≤0.5 wt.% Bi.

Relatively coarse-grained gold–silver alloy, several tens of μm in diameter, occurs within chalcopyrite, locally intergrown with Se-rich galena (up to 2.1 wt.% Se). Galena also forms corona-like inclusions

Table 2
Re–Os isotope data.

Sample	Weight (g)	Re (ng/g)	2s[a]	Os[b] (ng/g)	2s	^{187}Os (ng/g)	2s[a]	^{187}Re/^{188}Os	2s[a]	^{187}Os/^{188}Os	2s[c]
603/1	1.2020	298.5	3.4	0.19225	0.00266	1.4261	0.0200	7426	126	56.4	0.9
605/2	1.2000	123.3	1.3	0.00643	0.00028	0.5549	0.0042	91,714	3248	656.7	22.3
605/3	1.1990	64.18	0.77	0.00400	0.00016	0.2930	0.0025	76,683	2168	556.9	14.7
605/3	1.2000	63.61	0.79	0.00393	0.00027	0.2923	0.0027	77,456	3648	566.3	26.1
605/4	1.2010	62.50	0.70	0.00542	0.00031	0.2784	0.0023	55,121	2374	390.7	16.4
605/5	1.2020	60.91	0.52	0.00360	0.00029	0.2762	0.0023	80,835	4228	583.3	30.2
605/8	1.2020	50.30	0.63	0.00911	0.00038	0.2275	0.0020	26,416	960	190.1	6.5
1602/2	1.2000	77.69	0.87	0.00720	0.00041	0.3572	0.0027	51,606	2403	377.5	17.1
1611/2	1.2000	27.38	0.31	0.01013	0.00040	0.1258	0.0012	12,927	454	94.5	3.2
Blank 1	1.2000	0.0018	0.0006	0.00078	0.00002	0.0001					
Blank 2	1.2000	0.0022	0.0005	0.00093	0.00006	0.0001					
Blank average		0.0020	0.0006	0.00085							
603/1 R	1.1985	302.9	1.7	0.19230	0.00140	1.406	0.0080				
605/2 R	1.2158	124	0.7	0.00730	0.00060	0.5501	0.0029				
HLP	0.0110	283,908	1663			659.7	3.7				
HLP	0.0105	284,006	1960			657.2	4.3				

Sample	^{187}Re (ng/g)	2s[a]	187Os[d] (ng/g)	2s[a]	Model age (Ma)	2s[a]
603/1	187.6	2.12	1.3553	0.0212	432.0	8.3
605/2	77.50	0.82	0.5526	0.0031	426.5	5.1
605/3	40.34	0.48	0.2915	0.0020	432.2	6.0
605/3	39.98	0.49	0.2909	0.0023	435.1	6.4
605/4	39.28	0.44	0.2764	0.0019	420.9	5.5
605/5	38.28	0.33	0.2749	0.0018	429.5	4.7
605/8	31.62	0.40	0.2241	0.0016	424.0	6.1
1602/2	48.83	0.54	0.3546	0.0021	434.2	5.5
1611/2	17.21	0.19	0.1221	0.0010	424.3	5.9
HLP	283,908	1663	659.7	3.7	221.5	2.6
HLP	284,006	1960	657.2	4.3	220.6	2.8

^{187}Os (ng/g) is total ^{187}Os.
Certified age of HLP molybdenite standard is 221.4 ± 5.6 Ma.
Model ages are calculated with the ^{187}Re decay constant of 1.666×10^{-11} yr^{-1} (Smoliar et al., 1996). Uncertainty includes errors in ^{185}Re and ^{190}Os spike calibrations (2s), magnification with spiking, mass spectrometric measurement of isotopic ratios and uncertainty of decay constant 1.02%.
[a] 2s is total error.
[b] ^{187}Os is common Os (minus blank),
[c] 2s is mass error.
[d] ^{187}Os (ng/g) is radiogenic ^{187}Os.

surrounding gold grains within chalcopyrite (Fig. 8). Very small gold–silver inclusions, about 1 μm in diameter, occur in pyrite. The chemical composition of all gold–silver inclusions is remarkably constant (15–16 wt.% Ag) and corresponds to the stoichiometric formula of Au_3Ag. A multitude of Pb- and Ag-bearing tellurides, selenides, and bismuthides, typically about 1 μm in size, occur as very fine-grained inclusions in pyrite or at grain boundaries of pyrite–chalcopyrite. Rucklidgeite $(Bi,Pb)_3Te_4$, is relatively abundant and has 1–2 wt.% Se and ≤1 wt.% Ag. Altaite (PbTe), hessite (Ag_2Te), empressite (AgTe), volynskite ($AgBiTe_2$), and tellurobismuthite (Bi_2Te_3) were identified by electron microprobe. There are also many unnamed phases of the element association of Pb–Bi–Se–Te–S, such as Pb_3Se_2, $Pb_{10}(Te,Se)_3$, $Pb(Te,Se)_4$, PbSeS, $Pb_2(Te,Bi,Se)_3$, $Pb(Te,Bi,Se)_4$, Ag_3Te, $Ag(+Au)BiS_2$, and $(Ag,Pb)_3(Te,Bi)_2$.

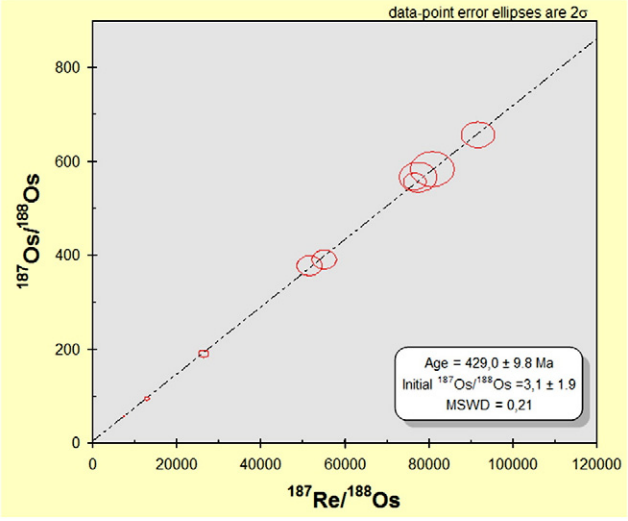

Fig. 10. ^{187}Re/^{188}Os–^{187}Os/^{188}Os isochron plot of bulk ore samples from the Dapingzhang stockwork ore. Model 1 solution on 9 points; errors are 2 sigma.
Plot and calculation based on ISOPLOT of Ludwig (2009).

The mineralogical composition is also expressed in the geochemistry of the ore samples, which exhibit a number of typical co-variation trends and metal-zonation features (Fig. 9a and b):

1. Arsenic, antimony, mercury, and silver, which are mostly bound to tetrahedrite–tennatite, are enriched in massive sulfide ore without hydrothermal overprint, i.e. in the distal ore.
2. Bismuth is exclusively enriched in stockwork ore. It is bound to rucklidgeite and to a number of other rare tellurides and selenides. This diagnostic feature is also known from feeder zones of the VHMS deposits in the Iberian Pyrite Belt (Marcoux et al., 1996).
3. Molybdenum and correlated rhenium are mineralogically expressed as erratic molybdenite in the deeper parts of the stockwork zone. Some molybdenum- and Re-rich samples have more than 100 ppb Pd and Pt (ESM, Table 2).
4. Gold and copper are particularly enriched in the stockwork ore and at the interface of the stockwork and massive sulfide ore (as much as >10 g/t Au and >10% Cu), but are also enriched to lesser degree in distal massive sulfide ore (as much as 1 g/t Au and 1% Cu), a feature also known from the Iberian Pyrite belt (Leistel et al., 1998).

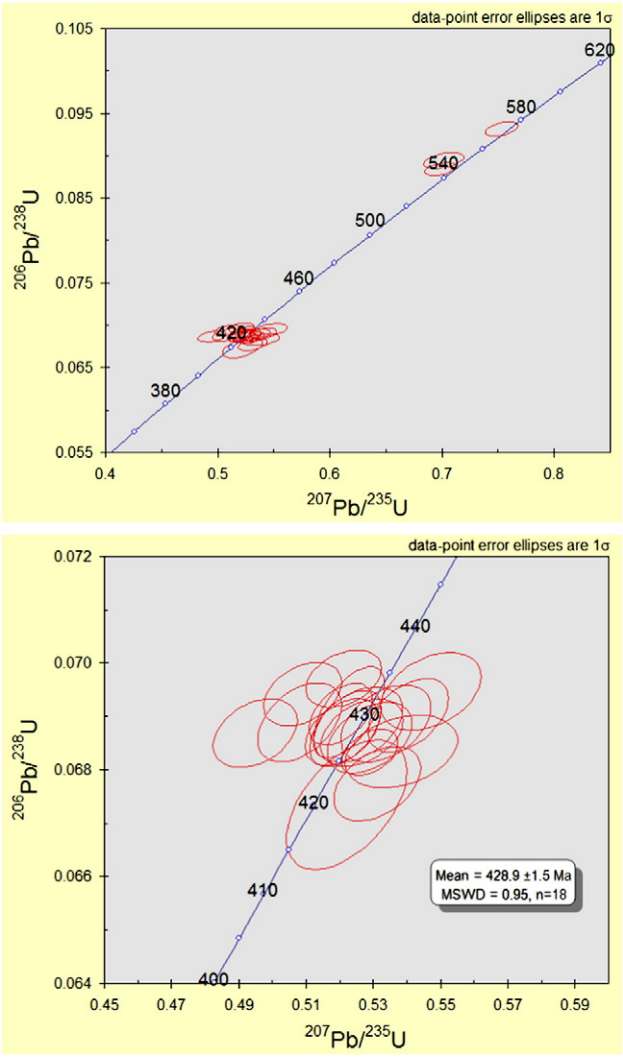

Fig. 11. U–Pb concordia plot for the mid-Silurian dacite sequence (sample Y-1).

The Ag/Au ratio in distal massive sulfide ore is about 1000, but <100 in stockwork ore where gold occurs as Au_3Ag alloy.

The metal zonation pattern is likely to reflect high-temperature fluid flow, probably of magmatic origin as supported by the elevated Bi and Te contents, through the stockwork/feeder zone, with dilution and cooling of the metal-rich hydrothermal plume by interaction with ambient seawater.

7. Re–Os dating of stockwork ore samples from Dapingzhang

The Re–Os isotope data on bulk-ore samples are shown in Table 2 and define a $^{187}Re/^{188}Os$–$^{187}Os/^{188}Os$ isochron of 429 ± 10 Ma (2σ, MSWD 0.21, initial $^{187}Os/^{188}Os$ 3.1 ± 1.9), i.e. a Middle Silurian age (Fig. 10). Common (i.e., non-radiogenic) Os is very low, and the absolute abundances of ^{187}Re and ^{187}Os also define an isochron within the error limits of the $^{187}Re/^{188}Os$–$^{187}Os/^{188}Os$ isochron. The initial $^{187}Os/^{188}Os$ of 3.1 ± 1.9 indicates a mainly crustal origin of the common osmium. The model ages for the nine individual samples range from 435 ± 6 to 424 ± 16 Ma and have a weighted average of 429 ± 4 Ma (Table 2).

8. U–Pb zircon dating of the Dapingzhang–Yinzishan dacite sequence

Eighteen U–Pb isotope measurements on zircon from dacite sample Y-1 (bulk-rock chemical data in ESM Table 2) gave an age of 428.9 ± 1.5 Ma (1σ, MSWD = 0.95), with a concordance of individual data points between 96 and 99% (Fig. 11, Table 3). Three zircons gave older ages between 546 ± 5 and 574 ± 4 Ma, which we interpret to represent inherited crystals. The U–Pb zircon age of 429 ± 3 Ma (2σ) coincides with the Re–Os age on Mo-enriched stockwork ore of 429 ± 10 Ma and proves synchroneity of dacite volcanism and hydrothermal ore formation.

9. Discussion of the mid-Silurian age of the dacite sequence and its significance for the early Paleozoic evolution of northern Gondwana

The dacite sequence and associated VHMS mineralization in the Dapingzhang anticline has been the subject of several geochronological studies with ambiguous results. There were several attempts of whole-rock Rb–Sr dating that gave scatterchrons between 511 ± 8 Ma (Zhong et al., 2000) and 236 ± 5 (Yang et al., 2000). Potassium–Ar data on chloritized dacite breccia gave ages between 317 and 295 Ma (Zhong et al., 2000). Our own data indicate that both the Sr and Nd isotope systems of the dacite sequence are disturbed (Table 1c). However, Zhong et al. (2000) published a Nd isochron age of 513 ± 40 Ma (n = 5), with $\varepsilon_{Nd}(t)$ 2.7 ± 0.8.

Liao (2002) and Dai et al. (2005) conducted a Sr isotope study on leachates of crushed hydrothermal quartz from the stockwork ore. The sampled material represents bulk fluid inclusions solutions and gave consistent $^{87}Sr/^{86}Sr$ ratios of 0.70836 ± 19 (n = 6). The data define an isochron of 118 ± 12 Ma, with an initial ratio of 0.708007 ± 37 (MSWD 0.46), which was interpreted as the age of formation of the Dapingzhang deposit. However, this age likely represents the age of most recent tectonic shearing and associated trapping of secondary fluid inclusions in brecciated quartz. In other words, the data reflect the Sr isotope composition of Early Cretaceous basinal brines, as Early Cretaceous seawater is distinctly less radiogenic ($^{87}Sr/^{86}Sr$ = 0.7074 ± 1; McArthur et al., 2001).

We have obtained the first reliable zircon U–Pb ages of the volcanic rocks at ca. 430 Ma, which is confirmed by Re–Os dating on molybdenum-rich bulk ore. This definitive age has significant implications for the understanding of the northern margin of Gondwana. The dacite–andesite sequence with minor basalt and rhyolite has a geochemical arc signature. The massive sulfide ore suggests a back-arc situation, and thus, an extensional domain within an overall contractional environment (Huston et al., 2010). This geotectonic interpretation has also been suggested earlier based on lithological studies (Feng et al., 2000; Feng and Helmcke, 2001) and is typical of most felsic rock-dominated VHMS deposits (Franklin et al., 2005).

The paleogeographic reconstruction for northern Gondwana in mid-Silurian times is shown in Fig. 12. The Simao block, which includes the Dapingzhang area, is part of the South China–Indochina composite terrane in modern SE Asia. The Early Paleozoic location of the Simao block is unknown, but it must be close to or part of the larger South China, Tarim, or Indochina blocks. The occurrence of both dacites and VHMS mineralization at Dapingzhang suggests that there was an active convergent margin in the mid-Silurian along the western part of NE Gondwana. The 430 Ma submarine dacite magmatism can best be interpreted as resulting from back-arc basin spreading. The mid-Silurian back-arc volcanic rocks are exposed only in the tectonic windows of the Dapingzhang area, but likely are present at depth across the modern Simao basin, possibly as far east as the Jinshajiang–Ailaoshan fault zone where basalt xenoliths of about 443–401 Ma have been found in 387–377 Ma ophiolite (Jian et al., 2009a, 2009b). East of the Jinshajiang–Ailaoshan zone, the South China block records the setting of a stable Early Paleozoic platform with shallow water carbonate deposition, with no evidence of continental rifting, back-arc volcanism, or Kuroko-style VHMS mineralization.

The formation of this back-arc basin during the mid-Silurian may be attributed to southward or eastward subduction along an active plate margin of northeastern Gondwana with hinge retreat leading

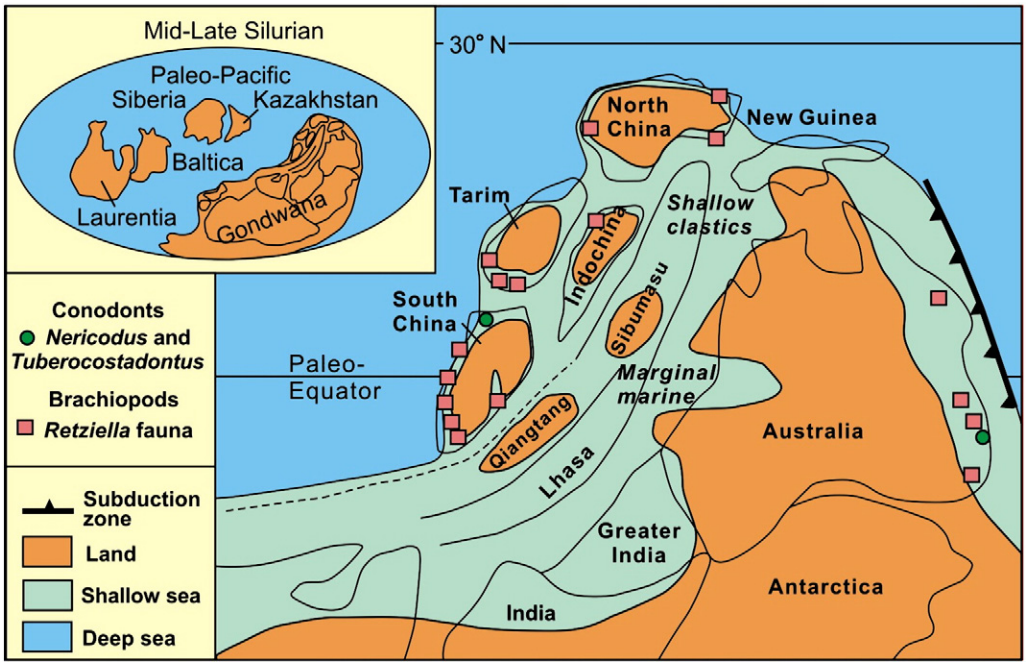

Fig. 12. Reconstruction of northeastern Gondwana for the mid- to late Silurian, showing the postulated positions of the East and Southeast Asian terranes, the distribution of land and sea, and the distribution of shallow-marine fossils (characterized by the *Retziella* brachiopod fauna) that illustrate Asia–Australia connections at that time. The South China, Tarim, Indochina and North China blocks are a group of continental fragments which separated from Indo-Australian Gondwana during the Devonian, with the Paleo-Tethys Ocean opening in between. The Dapingzhang area is in the Simao block (not located in the map) which is part of the larger Indochina or South China block. The mid-Silurian dacite sequence of the Dapingzhang massive sulfide deposit suggests a Paleo-Pacific subduction zone to the west of the paleo-South China or paleo-Indochina block, including an active continental margin.
From Metcalfe (2005).

to the opening of a basin, in a manner analogous to the Miocene rifting of the Ryukyu arc and opening of the present-day Okinawa Trough (Shinjo et al., 1999). Indications for Early Paleozoic rifting along the western margin of Indo-Australian Gondwana are also seen in major Early Paleozoic intracontinental basins along the modern NW shelf of Australia, and in Cambro-Ordovician deep water sedimentary rocks along the margins of the Tarim and Indochina blocks (Metcalfe, 1998, 2011). The reconstruction of the exact paleogeographic location of the Simao block within the Gondwana margin is not only difficult due to the complex amalgamation history of SE Asia, but also due to the Cenozoic overprint of the SE Asian terrain collage during the India–Asia collision which produced sinistral strike-slip displacements on the order of several hundred kilometers along the western margin of the South China block (Tapponnier et al., 1990; Wang and Burchfiel, 1997; Hennig et al., 2009). It appears likely that the mid-Silurian back-arc sequence of the Simao basin had a pre-Cenozoic position a few hundred km northwestward. Remnants of this paleo-active margin may still be found within the microcontinental

Table 3
U–Pb isotope data on zircon from sample Y-1.

Zircon spot	Pb total	^{232}Th	^{238}U	^{207}Pb/^{206}Pb	^{207}Pb/^{206}Pb	^{207}Pb/^{235}U	^{207}Pb/^{235}U	^{206}Pb/^{238}U	^{206}Pb/^{238}U	Rho	^{207}Pb/^{206}Pb	^{207}Pb/^{206}Pb	^{207}Pb/^{235}U	^{207}Pb/^{235}U	^{206}Pb/^{238}U	^{206}Pb/^{238}U	Concordance
	ppm	ppm	ppm		1 sigma		1 sigma		1 sigma		Age (Ma)	1 sigma	Age (Ma)	1 sigma	Age (Ma)	1 sigma	
Y1-01	10.02	30.9	111	0.0568	0.0010	0.5404	0.0097	0.0690	0.0006	0.4547	483	39	439	6	430	3	98%
Y1-02	23.39	82.3	256	0.0559	0.0007	0.5289	0.0068	0.0683	0.0004	0.4052	450	30	431	5	426	2	98%
Y1-03	10.10	38.2	113	0.0552	0.0009	0.5217	0.0087	0.0688	0.0006	0.5097	420	37	426	6	429	4	99%
Y1-04	7.37	20.9	85.8	0.0534	0.0010	0.5090	0.0094	0.0694	0.0005	0.3787	346	44	418	6	433	3	96%
Y1-05	9.08	27.4	105	0.0542	0.0010	0.5212	0.0091	0.0697	0.0004	0.3601	389	41	426	6	434	3	98%
Y1-06	6.62	21.7	78.0	0.0550	0.0009	0.5208	0.0090	0.0687	0.0005	0.4295	413	39	426	6	428	3	99%
Y1-07	8.26	38.2	96	0.0569	0.0012	0.5312	0.0105	0.0677	0.0006	0.4205	487	44	433	7	423	3	97%
Y1-08	7.85	28.1	89	0.0537	0.0011	0.5081	0.0102	0.0689	0.0006	0.4376	367	79	417	7	429	4	97%
Y1-09	8.30	32.4	91.1	0.0560	0.0011	0.5289	0.0103	0.0686	0.0005	0.4057	450	44	431	7	428	3	99%
Y1-10	16.19	67.3	173	0.0545	0.0008	0.5203	0.0077	0.0690	0.0005	0.4587	394	36	425	5	430	3	98%
Y1-11	9.54	37.6	94.6	0.0572	0.0013	0.5472	0.0122	0.0695	0.0006	0.3852	498	47	443	8	433	4	97%
Y1-12	11.78	58.9	126	0.0559	0.0011	0.5337	0.0109	0.0689	0.0006	0.4178	450	14	434	7	429	4	98%
Y1-13	8.05	28.3	72.2	0.0573	0.0009	0.6984	0.0112	0.0884	0.0006	0.4343	502	37	538	7	546	4	98%
Y1-14	8.30	27.8	77.2	0.0567	0.0012	0.7015	0.0145	0.0894	0.0008	0.4162	480	46	540	9	552	5	97%
Y1-15	16.39	101	138	0.0583	0.0009	0.7532	0.0121	0.0931	0.0007	0.4515	543	35	570	7	574	4	99%
Y1-16	9.02	44.3	111	0.0553	0.0011	0.5255	0.0108	0.0688	0.0006	0.4069	433	44	429	7	429	3	99%
Y1-17	7.47	25.7	92	0.0570	0.0014	0.5383	0.0136	0.0683	0.0006	0.3193	500	54	437	9	426	3	97%
Y1-18	7.08	26.0	86.4	0.0567	0.0016	0.5221	0.0146	0.0673	0.0010	0.5234	480	63	427	10	420	6	98%
Y1-19	10.71	43.8	125	0.0523	0.0011	0.4949	0.0102	0.0687	0.0005	0.3688	298	48	408	7	428	3	95%
Y1-20	23.03	136	267	0.0546	0.0007	0.5227	0.0087	0.0691	0.0007	0.6093	398	34	427	6	431	4	99%
Y1-21	9.97	45.4	113	0.0555	0.0010	0.5266	0.0100	0.0687	0.0005	0.3927	435	43	430	7	428	3	99%

collage of western Yunnan and the Tibetan Plateau where poorly-defined early Paleozoic subduction-related rocks are known (Zhu et al., 2013).

Supplementary data to this article can be found online at http://dx.doi.org/10.1016/j.gr.2012.12.018.

Acknowledgments

This study was initiated by a technical cooperation project between the German Geological Survey (Federal Institute for Geosciences and Natural Resources; BGR) and the Yunnan Bureau of Geology and Mineral Resources in 2002–2004. We thank Friedhelm Wellmer and Wengchang Li, the two Directors of the two institutions at that time, for their great interest and support.

Andao Du thanks Wenjun Qu and Fagang Zeng for analytical work in the Low-blank Re–Os lab in Beijing. Xinfu Xu thanks Liang Li for help at the LA-ICP-MS lab at the State Key Laboratory for Ore Deposit Geochemistry in Guiyang. Electron microprobe work in Clausthal was done by Galina Shcheka. Bernd Lehmann thanks Ruizhong Hu for help with this project and a grant from the Open Research Fund of the State Key Laboratory of Ore Deposit Geochemistry of China. We acknowledge discussions of the Re–Os data with Holly Stein. Editorial work by Richard Goldfarb and critical reading by Steven D. Scott and Kaihui Yang helped to improve the manuscript.

References

Briqueu, L., Bougault, H., Joron, J.L., 1984. Quantification of Nb, Ta, Ti and V anomalies in magmas associated with subduction zones. Petrogenetic implications. Earth and Planetary Science Letters 68, 297–308.

Dai, B.Z., Jiang, S.Y., Liao, A.L., 2005. Origin of hydrothermal ore-forming processes in the Dapingzhang polymetallic copper deposit in the Lanping–Simao basin, Yunnan Province. In: Mao, J.W., Bierlein, F. (Eds.), Mineral Deposit Research: Meeting the Global Challenge: Proceedings SGA Meeting, Beijing, vol. 1, pp. 739–742.

Du, A.D., Wu, S.Q., Sun, D.Z., Wang, S.X., Qu, W.J., Markey, R., Stein, H., Morgan, J., Malinovskiy, D., 2004. Preparation and certification of Re–Os dating reference materials: molybdenite HLP and JDC. Geostandard and Geoanalytical Research 28 (1), 41–52.

Eldridge, C.S., Barton Jr., P.B., Ohmoto, H., 1983. Mineral textures and their bearing on the formation of the Kuroko orebodies. Economic Geology Monographs 5, 241–281.

Faure, G., 1986. Principles of Isotope Geology. Wiley, 589 p.

Feng, Q.L., 2002. Stratigraphy of volcanic rocks in the Changning–Menglian belt in southwestern Yunnan, China. Journal of Asian Earth Sciences 20, 657–664.

Feng, Q.L., Helmcke, D., 2001. Late Paleozoic compressional deformation in the Simao region, southern Yunnan, P.R. of China. Newsletter on Stratigraphy 39, 21–31.

Feng, Q.L., Zhang, Z.F., Liu, B.P., Shen, S.Y., Zjang, W.M., Zhang, S.T., 2000. Radiolarian fauna from the Longdonghe Formation at the western margin of the Simao Massif and its geological significance. Journal of Stratigraphy 24 (2), 126–128.

Feng, Q.L., Shen, S.Y., Liu, B.P., Helmcke, D., Qian, X.G., Zhang, W.M., 2002. Permian radiolarians, chert and basalt from the Daxinshan Formation in Lancangjiang belt of southwestern Yunnan, China. Science in China (Series D) 45, 63–71.

Feng, Q.L., Chonglakmani, C., Helmcke, D., Ingavat-Helmcke, R., Liu, B.P., 2005. Correlation of Triassic stratigraphy between the Simao and Lampang–Phrae basins: implications for the tectonopaleogeography of Southeast Asia. Journal of Asian Earth Sciences 24, 777–785.

Franklin, J.M., 1996. Volcanic-associated massive sulphide deposits. In: Eckstrand, O.R., Sinclair, W.D., Thorpe, R.I. (Eds.), Geology of Canadian Mineral Deposit Types: Geology of Canada, 8, pp. 158–183.

Franklin, J.M., Gibson, H.L., Jonasson, I.R., Galley, A.G., 2005. Volcanogenic massive sulfide deposits. Economic Geology 100th Anniversary Volume, pp. 523–560.

Hennig, D., 2010. Magmatic evolution and platinum potential of SW Yunnan, China. Ph.D. thesis, Technical University of Clausthal, 249 p.

Hennig, D., Lehmann, B., Frei, D., Belyatsky, B., Zhao, X.F., Cabral, A.R., Zeng, P.S., Zhou, M.F., Schmidt, K., 2009. Early Permian seafloor to continental arc magmatism in the eastern Paleo-Tethys: U–Pb age and Nd–Sr isotope data from the souther Lancangjiang zone, Yunnan, China. Lithos 113, 408–422.

Heppe, K., 2006. Plate tectonic evolution and mineral resource potential of the Lancang River Zone, southwestern Yunnan, People's Republic of China. Geologisches Jahrbuch Sonderhefte SD 7, 1–159.

Heppe, K., Helmcke, D., Wemmer, K., 2007. The Lancang River Zone of southwestern Yunnan, China: a questionable location for the active continental margin of Paleotethys. Journal of Asian Earth Sciences 30, 706–720.

Huston, D.L., Pehrsson, S., Eglington, B.M., Zaw, K., 2010. The geology and metallogeny of volcanic-hosted massive sulfide deposits: variations through geological time and with tectonic setting. Economic Geology 105, 571–591.

Jacobsen, S.B., Wasserburg, G.J., 1980. Sm–Nd isotopic evolution of chondrites. Earth and Planetary Science Letters 50, 139–155.

Jian, P., Liu, D.Y., Kröner, A., Zhang, Q., Wang, Y.Z., Sun, X.M., Zhang, W., 2009a. Devonian to Permian plate tectonic cycle of the Paleo-Tethys orogen in southwest China (I): geochemistry of ophiolites, arc/back-arc assemblages and within-plate igneous rocks. Lithos 113, 748–766.

Jian, P., Liu, D.Y., Kröner, A., Zhang, Q., Wang, Y.Z., Sun, X.M., Zhang, W., 2009b. Devonian to Permian plate tectonic cycle of the Paleo-Tethys orogen in southwest China (II): insights from zircon ages of ophiolites, arc/back-arc assemblages and within-plate igneous rocks and generation of the Emeishan CFB province. Lithos 113, 767–784.

Kraume, E., 1955. Die Erzlager des Rammelsberges bei Goslar. Geologisches Jahrbuch Beihefte 18, 1–394.

Leistel, J.M., Marcoux, E., Deschamps, Y., Joubert, M., 1998. Antithetic behaviour of gold in the volcanogenic massive sulphide deposits of the Iberian Pyrite Belt. Mineralium Deposita 33, 82–97.

Li, G.Z., Li, C.S., Ripley, E.M., Kamo, S., Su, S.G., 2012. Geochronology, petrology and geochemistry of the Nanlinshan and Banpo mafic–ultramafic intrusions: implications for subduction initiation in the eastern Paleo-Tethys. Contributions to Mineralogy and Petrology 164, 773–788.

Liao, Q.L., 2002. Geochemical study of Cu–Pb–Zn polymetallic deposits from the Lanping–Simao basin, Yunnan. Unpublished Postdoc report, Nanjing University (in Chinese).

Liew, T.C., McCulloch, M.T., 1985. Genesis of granitoid batholiths of Peninsular Malaysia and implications for models of crustal evolution: evidence from a Nd–Sr isotopic and U–Pb zircon study. Geochimica et Cosmochimica Acta 49, 587–600.

Liu, Y.S., Gao, S., Hu, Z.C., Gao, C.G., Zong, K.Q., Wang, D.B., 2010. Continental and oceanic crust recycling-induced melt–peridotite interactions in the Trans-North China Orogen: U–Pb dating, Hf isotopes and trace elements in zircons from mantle xenoliths. Journal of Petrology 51, 537–571.

Ludwig, K.R., 2009. Isoplot/Ex3.Berkeley Geochronology Center (version 3.71.09.05.23nx).

Marcoux, E., Moelo, Y., Leistel, J.M., 1996. Bismuth and cobalt minerals as indicators of stringer zones to massive sulphide deposits, Iberian Pyrite Belt. Mineralium Deposita 31, 1–26.

McArthur, J.M., Howarth, R.J., Bailey, T.R., 2001. Strontium isotope stratigraphy: LOWESS version 3: best fit to the marine Sr-isotope curve for 0–509 Ma and accompanying look-up table for deriving numerical age. Journal of Geology 109, 155–170.

Mercier-Langevin, P., Hannington, M.D., Dubé, B., Bécu, V., 2011. The gold content of volcanogenic massive sulfide deposits. Mineralium Deposita 46, 509–539.

Metcalfe, I., 1998. Palaeozoic and Mesozoic geological evolution of the SE Asian region: multidisciplinary constraints and implications for biogeography. In: Hall, R., Holloway, J.D. (Eds.), Biogeography and Geological Evolution of SE Asia. Backbuys Publ., Leiden, pp. 25–41.

Metcalfe, I., 2005. Asia/South-East. In: Selley, R.C., Cocks, R.M., Plimer, I.R. (Eds.), Encyclopedia of Geology. Elsevier, pp. 169–196.

Metcalfe, I., 2006. Palaeozoic and Mesozoic tectonic evolution and palaeogeography of East Asian crustal fragments: the Korean Peninsula in context. Gondwana Research 9, 24–46.

Metcalfe, I., 2011. Tectonic framework and Phanerozoic evolution of Sundaland. Gondwana Research 19, 3–21.

Peng, T.P., Wang, Y.J., Fan, W.M., Liu, D., Shi, Y.R., Miao, L., 2006. SHRIMP zircon U–Pb geochronology of early Mesozoic felsic igneous rocks from the southern Lancangjiang and its tectonic implications. Science in China (Series D) 49, 1032–1042.

Rong, J.Y., Boucot, A.J., Su, Y.Z., Strusz, D.L., 1995. Biogeographical analysis of Late Silurian brachiopod faunas, chiefly from Asia and Australia. Lethaia 28, 39–60.

Sengör, A.M.C., Natal'in, B.A., Burtman, V.S., 1993. Evolution of the Altaid tectonic collage and Paleozoic crustal growth in Eurasia. Nature 364, 299–307.

Shinjo, R., Chung, S.L., Kato, Y., Kimura, M., 1999. Geochemical and Sr–Nd isotopic characteristics of volcanic rocks from the Okinawa Trough and Ryukyu Arc: implications for the evolution of a young, intracontinental back arc basin. Journal of Geophysical Research 104, 10591–10608.

Shirey, S.B., Walker, R.J., 1995. Carius tube digestion for low-blank rhenium–osmium analysis. Analytical Chemistry 67, 2136–2141.

Smoliar, M.I., Walker, R.J., Morgan, J.W., 1996. Re-Os ages of group IIA, IIIA, IVA, and IVB iron meteorites. Science 271, 1099–1102.

Steiger, R.H., Jäger, E., 1977. Subcommision on geochronology: convention on the use of decay constants in geo- and cosmochronology. Earth and Planetary Science Letters 36, 359–362.

Swinden, H.S., 1996. The application of volcanic geochemistry to the metallogeny of volcanic-hosted sulphide deposits in central Newfoundland. Short Course Notes, 12. Geological Association of Canada, pp. 329–358.

Tapponnier, P., Lacassin, R., Leloup, P.H., Schärer, U., Zhong, D.L., Wu, H.W., Liu, X.H., Ji, S.C., Zhang, L.S., Zhong, J.Y., 1990. The Ailao-Shan/Red River metamorphic belt: Tertiary left-lateral shear between Indochina and South China. Nature 343, 431–437.

Wang, E.C., Burchfiel, B.C., 1997. Interpretation of Cenozoic tectonics in the right-lateral accomodation zone between the Ailaoshan Shear Zone and the Eastern Himalayan Syntexis. International Geology Review 39, 191–219.

Winchester, J.A., Floyd, P.A., 1977. Geochemical discrimination of different magma series and their differentiation products using immobile elements. Chemical Geology 20, 325–343.

Yang, K.H., Scott, S.D., Mo, X.X., 1999. Massive sulfide deposits in the Changning–Menglian back-arc belt in western Xunnan, China: comparison with modern analogues in the Pacific. Exploration and Mining Geology 8, 211–231.

Yang, Y.Q., et al., 2000. Geological setting, metallogenic conditions and prediction of massive sulfide copper deposits in the volcanic belt of the southern Lancangjiang region, Yunnan province. Unpublished report, Institute of Mineral Deposits, Chinese Academy of Geological Sciences, and Number 5 Geological Brigade, Yunnan Bureau of Geology and Mineral Resources, Beijing and Kunming, 1–178 (in Chinese).

YBGMR Yunnan Bureau of Geology and Mineral Resources, 1990. Regional geology of Yunnan province. Geological Memoir Series, 1 (21). Geological Publishing House, Beijing.
YBGMR <Yunnan Bureau of Geology and Mineral Resources> 2001. Geological map 1:200,000 of Dapingzhang-Jako area. No. 5 Geological Brigade, Simao/Kunming.
Yui, S., 1983. Textures of some Japanese Besshi-type ores and their implications for Kuroko deposits. Economic Geology Monograph 5, 231–240.
Zhang, R.Y., Cong, B.L., Maruyama, S., Liou, J.G., 1993. Metamorphism and tectonic evolution of the Lancang paired metamorphic belts, south-western China. Journal of Metamorphic Geology 11, 605–619.
Zhong, D.L., 1998. The Paleotethys Orogenic Belt in West of Sichuan and Yunnan. Science Publishing House, Beijing.
Zhong, H., Hu, R.Z., Ye, Z.J., Tu, G.Z., 2000. Isotope geochronology of Dapingzhang spilite–keratophyre formation in Yunnan Province and its geological significance. Science in China (Series D) 43, 200–207.
Zhu, D.C., Zhao, Z.D., Nu, Y.L., Dilek, Y., Hou, Z.Q., Mo, X.X., 2013. The origin and pre-Cenozoic evolution of the Tibetan Plateau. Gondwana Research. 23 (4), 1429–1454 http://dx.doi.org/10.1016/j.gr.2012.02.002.